An improved method for the seismic design of anchored steel sheet pile walls

by V. Giorgio Caputo[a], Riccardo Conti[b], Giulia M. B. Viggiani[c], Cécile Prüm[d]

[a]PhD Student, Niccolò Cusano University, Rome, Italy.
e-mail: giorgio.caputo@unicusano.it

[b]Associate Professor, Niccolò Cusano University, Rome, Italy.
e-mail: riccardo.conti@unicusano.it

[c]Full Professor, Cambridge University, Cambridge, United Kingdom.
e-mail: gv278@cam.ac.uk

[d]Senior Research Engineer, ArcelorMittal, Esch-sur-Alzette, Luxembourg
e-mail: cecile.prum@arcelormittal.com

Contact Author:
Giorgio Caputo
Università Niccolò Cusano
Via Don Carlo Gnocchi, 3 - 00166 Roma, ITALY
e-mail: giorgio.caputo@unicusano.it

Abstract

This paper describes a new pseudo-static approach for an efficient seismic design of anchored steel sheet pile (ASSP) walls supported by shallow passive anchorages. As for other retaining structures, energy dissipation during strong earthquakes, leading to reduced inertia forces, can be achieved by allowing the activation of ductile plastic mechanisms. To this end, a robust method is required to identify all the possible yielding mechanisms and to guarantee the desired strength hierarchy. It is shown that dissipative mechanisms for ASSP walls correspond either to the local attainment of the soil shear strength in the supporting soil and around the anchor, or in the activation of a log-spiral global failure surface. A new limit equilibrium method is proposed to compute the critical acceleration of the system, corresponding to the actual mobilization of its strength, and the maximum internal forces in the structural members. Theoretical findings are validated against both existing dynamic centrifuge data and the results of original pseudo-static and fully dynamic numerical analyses.

Keywords:

Anchored retaining walls, Seismic design, Limit equilibrium methods, Global failure, Anchor capacity, Earth pressure

1. INTRODUCTION

Anchored steel sheet pile (ASSP) walls are complex retaining structures consisting of multiple structural elements, including the retaining wall, the tie rods and the anchors, interacting with one another and with the surrounding soil. Shallow passive anchorages, in the form of continuous sheet pile walls, are usually preferred to concrete walls and to grouted anchors, due to their convenience in implementation, particularly in port structures.

The seismic design of these structures must address essentially two requirements:

(1) verify that the embedment depth of the wall and the anchor system are such that the displacements induced by the design earthquake will be lower than an admissible threshold (geotechnical design);

(2) verify that the structural members (wall section and tie rods) can sustain the maximum internal forces induced by the design earthquake (structural design).

In current design practice, ASSP walls are usually designed using simple calculation tools, based on Limit Equilibrium (LE) methods or sub-grade reaction models. The same methods can be used, at least in principle, for the seismic design of ASSP walls using a pseudo-static approach (Neelakantan *et al.*, 1992; Zeng & Steedman, 1993; Ebeling & Morrison, 1993; Anderson *et al.*, 2008; Becci & Carni, 2014). However, they tend to yield moderately to highly over-conservative design, depending on the wall flexibility, the overall strength of the system, and assumptions on both the seismic action and the stress distribution into the soil.

By using numerical finite difference (FD) and finite element (FE) analyses it is possible to account for the dynamic soil-structure interaction and obtain more economical design solutions (Gazetas *et al.*, 2016; Gong *et al.*, 2019). However, numerical modelling of geotechnical systems under dynamic conditions is rather complex and not always readily accessible for the practicing engineer, requiring careful consideration of many factors, including *e.g.*, the selection of representative acceleration time histories, the definition of suitable boundary conditions and the choice of an adequate constitutive model for the soil.

In recent years, new design approaches have started to be explored for the performance-based seismic design of retaining structures. These are based on the idea that, during an earthquake, a retaining structure can experience permanent displacements, provided that the overall behaviour of the system is ductile and the associated damage does not exceed some allowable threshold, defined on the basis of a given required performance level (PIANC, 2001). Within this framework, the horizontal permanent displacement of the retaining structure, which is taken as a performance indicator of the whole system, is usually computed using Newmark's sliding block procedure (Newmark, 1965; Richards & Elms, 1979). In this method, the critical acceleration, *i.e.*, the acceleration corresponding to the full mobilization of the strength of the system, is key both to compute the permanent displacements experienced by the wall and to its structural design, as it defines the maximum internal forces that the structure may ever experience during any earthquake (Callisto, 2014; Conti *et al.*, 2014). The critical acceleration is usually computed using pseudo-static approaches, by means of either limit equilibrium methods or limit analysis, taking into account all the possible plastic mechanisms for the soil-wall system (Kloukinas *et al*., 2015; Conti & Caputo, 2019).

Application of Newmark's procedure to ASSP walls is still an open issue, given the multiple factors affecting the seismic behaviour of these structures (Neelakantan *et al.*, 1990; Lai, 1998; Fusco *et al*., 2019, Caputo *et al.*, 2019), such as *e.g.*, the wall flexibility and the embedment depth, altering the stress distribution around the main wall; the layout of the wall, the tie-rod and the anchor plate, governing the possible occurrence of different plastic mechanisms within the soil-wall system; the presence of water in the backfill and in front of the wall, inducing additional hydrodynamic forces into the system and possibly leading to pore pressure build-up within the soil.

This paper deals with some of the above issues**,** trying to provide insight into the physical mechanisms affecting the critical acceleration of ASSP walls and to establish a basis for a more efficient design procedure. In particular, a new pseudo-static LE method is presented for the computation of: (i) the maximum internal forces in the structural members; (ii) the anchor capacity; and (iii) the pseudo-static accelerations inducing local or global plastic mechanisms within the soil interacting with the

retaining structure. Moreover, a strength-hierarchy approach is proposed for the evaluation of the critical acceleration of the soil-anchor-wall system.

Theoretical findings are validated against both dynamic centrifuge tests on reduced scale physical models and pseudo-static and dynamic numerical FD analyses. At this stage, only dry sand is considered, neglecting any effects of pore pressure build-up during shaking.

2. PROPOSED METHOD

A rational approach to the seismic design of ASSP walls should contemplate all the possible yielding mechanisms of the system in order to achieve the desired strength hierarchy and to control the potential occurrence of damage under the design earthquake (PIANC, 2001). In this respect, ASSP walls are designed in order to avoid failure of the structural connections between the tie rod and the walls, which would lead to a brittle failure of the system, and yielding of both the tie rod and the main wall, which would be difficult to repair (JPHA, 1991; Ebeling & Morrison, 1993). In other words, typically, their seismic design does not rely upon the ductility of the structural members.

All other possible plastic mechanisms for these retaining systems involve a full mobilization of the shear strength in the soil. Three failure mechanisms can be identified, each activated by a given acceleration ($a_i = k_i g$):

1) attainment of the anchor capacity, corresponding to which the wall is expected to rotate around a point close to the toe (anchor failure, k_{AF});
2) complete mobilization of the soil passive strength below dredge level, leading to a progressive rotation of the wall around the tie rod connection (toe failure, k_{TF});
3) activation of a global plastic mechanism, involving both the wall, the anchor plate and the soil volume interacting with them (global failure, k_{GF}).

Once the accelerations corresponding to each mechanism are computed, following *e.g.*, a pseudo-static approach, then the critical acceleration of the system ($a_c = k_c \cdot g$) can be simply defined as:

$$a_c = \min_i(a_i) \quad (1)$$

127

128 *2.1 Contact stress distribution for the main wall*

129 For a given value of the pseudo-static coefficient, k_h, the stress distribution at the contact between the
130 soil and the main wall depends on the constraint imposed by the anchor and the bending stiffness of
131 the wall, controlling the amount of permanent deformations that the wall may undergo before a plastic
132 mechanism is activated. For passive anchorages, which need a certain amount of displacement to
133 activate the required resistance, the progressive mobilisation of soil passive strength is always initially
134 associated with a rotation of the main wall around a pivot point close to the toe, just as in the case of
135 cantilever walls (Zeng & Steedman, 1993; Gazetas *et al*., 2016). Based on these considerations, a
136 pseudo-static LE method is proposed for computing the soil-wall horizontal contact stress
137 distribution, inspired by the work carried out by Conti & Viggiani (2013) and Conte *et al*. (2017) on
138 embedded cantilever walls.

139 Figure 1a shows the assumed net earth pressure profile, referring to an ASSP wall (retained height H,
140 embedment depth D), retaining a cohesionless backfill (unit weight γ, friction angle ϕ', soil-wall
141 friction angle δ). On the retained side, the soil is in active limit state down to D^*; along the same
142 depth, the soil passive strength is fully mobilised in the supporting soil. Mononobe-Okabe closed
143 form solution (Okabe, 1924, Mononobe & Matsuo 1929) was used to compute the pseudo-static
144 active earth pressure coefficient (K_{AE}), while the lower-bound solution proposed by Lancellotta
145 (2007), which is inherently conservative, was used to compute the pseudo-static passive earth
146 pressure coefficient (K_{PE}).

147 At larger depths, contact pressures are no longer related to a limit state condition of the soil. For the
148 sake of simplicity, it is assumed that: (i) the net pressure varies linearly up to the toe of the wall, being
149 null at the pivot point, D_0; and (ii) the net pressure at the toe is equal to the value computed ad depth
150 D^*. Under these assumptions, the proposed diagram is completely defined once the depth D^* and the
151 anchor force T_a are known. These quantities can be easily computed from the two equilibrium
152 equations of the wall.

153

154 *2.2 Comparison with conventional approaches and validation*

155 In this section, the pseudo-static LE method is compared with two approaches conventionally adopted
156 in the design practice, both assuming a linear distribution of the soil-wall contact stress. The
157 corresponding net pressure diagrams are shown in Figure 2.

158 According to the first method (M1 in Figure 2a), the soil is in active limit conditions on the retained
159 side, while a constant fraction $1/SF_P$ of the soil passive strength is mobilised in front of the wall
160 (Neelakantan *et al.*, 1992). This diagram, which is compatible with a rotation of the wall around the
161 anchor level, is completely defined by the two unknowns T_a and SF_P.

162 The second method (M2 in Figure 2b) assumes that limit conditions are fully attained in the soil, as
163 a result of a rigid rotation of the wall around a pivot point close to the toe (Zeng & Steedman, 1993).
164 The retained soil is in active limit state down to the pivot point and in passive limit state below this
165 depth, while the supporting soil is in passive limit state down to D_0, and in active limit state below
166 the rotation point. In this case, the resulting net pressure distribution is completely defined by the two
167 unknowns T_a and D_0.

168 The evolution of the contact stress distribution with increasing k_h and the resulting internal forces, as
169 predicted by the three methods, are synthetically depicted in Figure 3, with reference to a typical
170 layout of an ASSP wall ($\gamma = 20$ kN/m^3, $\phi' = 35°$, $\delta = \phi'/3$, $D/H = 0.5$, $b/H = 0.1$). More in detail,
171 Figure 3 shows: (a) the amount of soil passive strength mobilised in front of the wall, defined in terms
172 of the ratios D^*/D (proposed method), $1/SF_P$ (method M1) and D_0/D (method M2); (b) the normalised
173 axial force in the tie rod, $T_a(k_h)/T_a(k_{TF})$; and (c) the maximum normalised bending moment in the wall,
174 $M_{max}(k_h)/M_{max}(k_{TF})$. The results are shown as a function of the ratio k_h/k_{TF}, where k_{TF} is the pseudo-
175 static seismic coefficient corresponding to which the passive strength in front of the wall is fully
176 mobilised, which is the same for all three methods. For a given value of the ratio k_h/k_{TF}, method M1
177 predicts a lower mobilisation of the soil passive resistance and, consistently, higher anchor force and
178 bending moment compared to the other two methods. On the other hand, method M2 always provides

179 D_0/D values close to unity, thus implying that the available passive strength is almost completely
180 mobilised even under small pseudo-static accelerations. This result leads invariably to lower values
181 of the predicted anchor force and maximum bending moment, compared to the proposed method.
182 The predictive capabilities of the three methods were assessed with reference to the experimental data
183 presented by Zeng & Steedman (1993), referring to a dynamic centrifuge test carried out on a reduced
184 scale model of an anchored retaining wall embedded in a uniform layer of dry sand. The excavation
185 and the embedment depth at prototype scale were equal to H = 7.2 m and D = 2.4 m, respectively.
186 Horizontal tie rods were used to connect the wall with the anchor plate ($b = b_A$ = 1.6 m), both
187 modelled using aluminium sheets. Leighton Buzzard 52/100 sand was used, reconstituted at a relative
188 density of D_R = 82%, corresponding to an estimated peak friction angle ϕ'_p = 45°.
189 The comparison between experimental data and theoretical predictions is provided with reference to
190 the static condition and two earthquakes, characterised by different values of the maximum recorded
191 soil acceleration, a_{max}/g = 0.06 and a_{max}/g = 0.135. In LE calculations, a friction angle δ = 12° was
192 assumed at the contact between the soil and the wall, as measured by Madabhushi & Zeng (2007).
193 For the sole method M2, the internal forces were computed using also δ = 0°, in order to provide a
194 direct comparison with the LE results published by Zeng & Steedman (1993).
195 Figure 4 shows the measured bending moment distributions in the wall, together with the results
196 provided by the three LE methods. Moreover, for the same cases, Figure 5 reports the values of the
197 axial force in the tie rods, as a function of k_h. As apparent, the proposed method is in very good
198 agreement with the experimental data, while the other methods tend to under- or over-predict the
199 structural internal forces, depending on the assumption on the contact stress distribution below dredge
200 level. Method M2, in conjunction with δ = 0°, also provides a very good estimate of the experimental
201 data. However, this result is of minor relevance in the design practice, where any LE method will be
202 used together with a realistic assumption on the soil-wall contact friction angle.
203
204 *2.3 Anchor capacity*

For a given k_h, Figure 1b shows the contact stress distribution assumed to compute the seismic capacity of the anchor, *i.e.*, the axial force (T_{lim}) inducing a plastic mechanism within the soil-anchor system. It is assumed that the soil strength is fully mobilised due to an outward rotation of the anchor plate and the corresponding contact stresses are derived under the assumptions of rigid plate and rigid perfectly plastic soil behaviour, which hold for typical values of the length of the anchor plate (H_A < 4-5 m). Consistently, passive earth pressures develop above the pivot point in front of the anchor plate and below H_0 on the back, while active earth pressures develop below the pivot point in front of the anchor plate and above H_0 on the back. The two unknowns T_{lim} and H_0, which define completely the contact pressure diagram, are computed from the two equilibrium equations of the anchor plate.

The position of the pivot point, H_0, and the maximum allowable axial force, T_{lim}, depend on the ratio b_A/H_A, representing the eccentricity of the anchor force. As an example, Figure 6 shows the maximum normalised allowable force, $T_{lim}/\gamma H_A^2$, as a function of k_h, for different values of b_A/H_A (c = 0, H_A = 3.2 m, γ = 20 kN/m^3, ϕ' = 35°, $\delta = \phi'/3$). As expected, T_{lim} increases with increasing b_A/H_A, with the upper bound provided by the condition b_A/H_A = 2/3, corresponding to which a pure triangular contact stress distribution is obtained.

2.4 Plastic mechanisms

According to the proposed LE method, Figure 7 shows the earth pressure distribution at the onset of each of the three possible plastic mechanisms: (a) toe failure ($D^* = D$); (b) anchor failure ($T_a = T_{lim}$); and (c) global failure. Inertia forces on the walls can be neglected, since their mass is relatively small compared to that of the interacting soil.

Following the original idea by Littlejohn (1972), recently applied also by Callisto & Del Brocco (2015) to grouted anchors, the global mechanism consists in a log-spiral failure surface extending from the pivot point of the main wall, with an angle $\alpha_{AE}(k_h)$ on the horizontal, to the tip of the anchor plate. In order to define completely the geometry of the log-spiral, it is assumed that $\alpha_{AE}(k_h)$

corresponds to the inclination of Mononobe-Okabe active soil wedge. Under the further assumption of a rigid rotation of the two walls and of the soil delimited by the failure surface around the centre (O) of the log-spiral, the forces relevant for the moment equilibrium of the system are displayed in Figure 7c. Accordingly, the pseudo-static yield acceleration a_{GF} is the one corresponding to which the driving moment matches the resisting one.

The two local plastic mechanisms are mutually exclusive, *i.e.*, a full attainment of the soil shear strength can be reached by either toe or anchor failure, depending on the seismic capacity of the anchor. To highlight this point, Figure 8 illustrates the evolution of: (a) the anchor force required for the stability of the retaining wall T_a, the anchor resistance T_{lim}, and (b) the ratio D^*/D, as a function of k_h. With increasing k_h, two limiting situations are possible:

(1) in the case of a weak anchor, local attainment of the anchor capacity ($T_a = T_{lim}$ at $k_h = k_{AF}$) precedes complete mobilization of the soil passive strength; therefore, in this case we have $D^*/D < 1$;

(2) for a strong anchor, complete mobilization of the soil passive strength below dredge level ($D^*/D = 1$ at $k_h = k_{TF}$) is achieved before anchor capacity is attained, for $T_a < T_{lim}$.

2.5 Critical acceleration and theoretical parametric study

An extensive parametric study was carried out to identify the most likely plastic mechanisms, for realistic layouts of ASSP walls. To this end, dimensional analysis was preliminarily adopted to derive the dimensionless parameters relevant for the design of ASSP walls (see Appendix), *i.e.*, ϕ', b/H, D/H, H_A/H, L/H, $SF_A = T_{lim}/T_a$ and $SF_L = L/L_{min}$, where L_{min} is the minimum tie rod length required to avoid overlapping of the active and passive soil wedges behind the main wall and in front of the anchor plate, respectively (under static conditions). In addition to these, the seismic capacity of the anchor is further affected by the dimensionless ratios c/H and b_A/H_A, the latter clearly related to the ratio b_A/b defining the inclination of the tie rods.

Four different soils (ϕ' = 25°, 30°, 35° and 40°), four anchor positions (b/H = 0.1, 0.2, 0.3 and 0.4) and two different tie rod inclinations (b_A/b = 1-1.5) were considered in the parametric study. Moreover, two values were considered for SF_L (1.1-1.5), while a typical value of SF_A = 2.5 was adopted, together with a constant ratio c/H = 0.05. The results are summarised in Figure 9, showing the computed critical acceleration as a function of b/H, for different values of ϕ' and for: (a) b_A/b = 1 and SF_L = 1.1; (b) b_A/b = 1 and SF_L = 1.5; and (c) b_A/b = 1.5 and SF_L = 1.5. As a general result, k_c increases both with increasing ϕ' and with increasing b/H, irrespective of the plastic mechanism activated within the system, except for the case of toe failure. The length of the tie rods affects strongly the critical mechanism, which corresponds always to a global failure for SF_L = 1.1. On the contrary, for SF_L = 1.5, an increasing b_A/b ratio (*i.e.*, an increasing inclination of the tie rod) leads to a stronger anchor, with the double effect of: (i) making generally the toe failure the most likely local plastic mechanism and (ii) increasing k_c in the case of a global failure.

3. NUMERICAL ANALYSES

The proposed theoretical model was validated against pseudo-static and dynamic numerical analyses, carried out in plane-strain conditions using the FD code FLAC v.5 (Itasca, 2005).

3.1 ASSP wall layouts

As shown in Table 1, four layouts were considered, all referring to an ASSP wall with H = 10 m, embedded in a homogeneous sand layer (ϕ' = 35°, γ = 20 kN/m^3). Case 1 is the reference layout, with typical dimensions derived from a conventional static design procedure (b/H = 0.1, D/H = 0.4, b_A/b = 1, c/H = 0.05, H_A/H = 0.3, L/H = 2.1). The corresponding critical plastic mechanism is a local failure of the anchor, with a critical acceleration of $a_c = a_{AF}$ = 0.13 g. The other layouts were chosen to emphasize the influence of the three dimensionless groups b_A/H_A, L/H and D/H on the overall seismic behaviour and on the expected critical plastic mechanism.

Inclined tie rods are introduced in case 2, with a reduced eccentricity of the tie rod connection at the anchor plate (increased b_A/H_A ratio). This solution increases substantially the capacity of the anchor and, consistently, a global plastic mechanism is expected, with a larger value of the critical acceleration ($a_c = a_{GF} = 0.22\ g$). Shorter tie rods are used in case 3 (reduced L/H ratio), but always compatible with a safe static design of the wall-anchor system. In this case, the reduced distance between the wall and the anchor plate makes the global mechanism the critical one ($a_c = a_{GF} = 0.08\ g$). Finally, case 4 is characterised by a larger D/H ratio, which does not alter the nature of the plastic mechanism but increases the predicted critical acceleration ($a_c = a_{AF} = 0.15\ g$).

3.2 Numerical model

Figure 10 shows a detail of the mesh adopted in the analyses. The depth and width of the numerical domain were selected not to affect the behaviour of the soil-wall-anchor system during the pseudo-static and dynamic stages. A symmetric domain was examined, with two facing identical ASSP walls placed at sufficient distance not to interact with one another.

The soil was modelled as an elastic-perfectly plastic material, with a Mohr-Coulomb failure criterion ($\gamma = 20$ kN/m^3, $\phi' = 35°$, $c' = 0$ kPa) and a non-associated flow rule ($\psi = 0°$). A constant Poisson's ratio was used ($\nu = 0.2$), while the shear modulus was given by $G = 10000\sqrt{p'}$(kPa), where p' is the mean effective stress. During the dynamic stage, a hysteretic soil model available in the FLAC library (sig3) was used to introduce nonlinearity and energy dissipation along stress paths within the yield surface (Conti *et al*., 2014). The corresponding constitutive parameters ($a = 1.0$, $b = -0.6$, $x_0 = -1.5$) were calibrated based on the shear modulus degradation and damping curves suggested by Vucetic & Dobry (1991) for cohesionless soils.

The main wall and the anchor plate were modelled as elastic beams with mechanical, geometrical and physical properties corresponding to those of an AZ24 profile (unit weight $\gamma = 60$ kN/m^3, cross-sectional moment of inertia $I = 5.582\times10^{-4}$ m^4/m, Young's modulus $E = 210$ GPa, $\nu = 0.3$). Elastic cable elements were used to model the tie rod (unit weight $\gamma = 78.5$ kN/m^3, diameter $d = 45$ mm/m,

307 E = 210 GPa, ν = 0.3). Finally, elastic–perfectly plastic interfaces were introduced between the wall
308 and the grid nodes, with a very large normal and shear stiffness ($k_n = k_s = 2\times10^7$ kN/m) and a Mohr-
309 Coulomb yield criterion ($\delta = \phi'/3$, $c' = 0$ kPa).
310 The analyses were performed in two stages. The initial static stage was modelled in successive steps,
311 under sole gravitational loads, in order to reproduce the backfilling construction procedure. Standard
312 static constraints were applied at the model boundaries, *i.e.*, zero horizontal displacements along the
313 vertical sides and fixed nodes at the base of the mesh.
314 After the static stage, in the pseudo-static analyses a uniform body force, defined as a fraction k_h of
315 the gravitational acceleration, was applied in the horizontal direction. The pseudo-static coefficient
316 was gradually increased until equilibrium could no longer be reached and a plastic mechanism
317 appeared within the soil-wall system (Conti & Caputo, 2018).
318 In the dynamic analyses, instead, the seismic input was applied to the bottom nodes of the mesh, as a
319 horizontal acceleration, while standard periodic constraints were applied to the lateral boundaries
320 (Conti *et al*., 2014). Figure 11 shows (a) the acceleration time histories and (b) the corresponding
321 Fourier amplitude spectra of the applied signals, all recorded on rock outcrop during real earthquakes.
322 Table 2 summarises the corresponding ground motion parameters, *i.e.*, peak ground acceleration,
323 *PGA*, velocity, *PGV*, and displacement, *PGD*; dominant frequency, f_d; mean frequency, f_m; Arias
324 intensity, I_a; and duration $T_{5\text{-}95}$. These inputs were chosen to cover a significant range of amplitudes
325 and frequency content.
326
327 **4. DISCUSSION OF RESULTS**
328 *4.1 Plastic mechanisms*
329 Figure 12 shows, for all layouts, the contours of shear strains computed in the pseudo-static analyses
330 at the onset of the critical condition, together with the corresponding values of the critical coefficient.
331 The active and passive slip surfaces provided by Mononobe-Okabe solution and the log-spiral surface
332 predicted by the proposed method are also reported for comparison. Theoretical and numerical values

333 of the critical acceleration are in very good agreement. Moreover, shear strains tend always to develop
334 between the two walls, moving from the toe of the main wall to the anchor plate, as a result of the
335 close connection between the local formation of plastic zones and the possible development of a
336 global plastic mechanism within the system.
337 On the one hand, the high concentration of shear strains around the anchor wall indicates an anchor
338 failure in cases 1 and 4 (Figure 12a, d), where both an active soil wedge behind the main wall and a
339 passive wedge in front of the anchor plate are clearly visible (even though Mononobe-Okabe solution
340 tends to over-predict the extension of the soil volume in passive limit state condition). On the other
341 hand, no active and passive slip surfaces developed between the walls in case 2 (Figure 12b), where
342 the shape of the global failure surface is in very good agreement with the predicted log-spiral. Finally,
343 case 3 (Figure 12c) exhibits an intermediate behaviour, since the weak anchor condition allows the
344 formation of plastic zones close to the structural members, even in the presence of a global critical
345 mechanism.
346
347 *4.2 Contact stresses and internal forces*
348 A further comparison between numerical pseudo-static results and theoretical predictions is provided
349 in Figure 13, referring to cases 1 and 2, in terms of contact pressure distributions and internal forces
350 in the structural members.
351 With increasing pseudo-static acceleration, the active pressures behind the main wall increase while
352 the available passive strength decreases and, consequently, equilibrium of the wall requires a deeper
353 mobilization of the passive resistance below dredge level. This trend is well predicted by the proposed
354 LE method, both qualitatively and quantitatively (Figure 13a, d). Similarly, the evolution of contact
355 stresses around the anchor plate confirms that the critical condition is related to full attainment of the
356 anchor capacity only in case 1, as predicted by the theoretical approach (Figure 13b, e).
357 On the other hand, the assumed linear active distribution behind the wall cannot capture the
358 concentration of soil pressures close to the anchor level, due to the local restraint imposed by the tie

rod. However, as the amount of constraint depends on the displacements of the anchor system, this stress concentration is less pronounced in case 1 (anchor failure condition) and vanishes at the onset of the critical condition, where the distribution in the upper part of the retained soil becomes approximately linear in both layouts. As a result, for $k_h < k_c$, the theoretical LE method tends to under-predict the axial force in the tie rods and slightly over-predict the bending moment in the main wall (Figure 13c, f). For $k_h = k_c$, instead, theoretical and numerical values of the maximum internal forces are in fairly good agreement in case 1, while numerical results are substantially under-predicted in case 2.

The latter observation stems from the fact that, when the critical condition corresponds to a global plastic mechanism ($a_c = a_{GF}$), the strength in the retained soil is not yet fully mobilised and the structural internal forces are actually a result of a soil-structure interaction problem (Callisto & Del Brocco, 2015). Nonetheless, taking into consideration that maximum (ever possible) internal forces must be compatible with the available soil strength, their values can still be estimated within a LE framework, considering the local plastic mechanism characterised by the lower value of yield acceleration. In order to make this point clearer, Figure 14 shows, for case 2, the numerical contact pressure and bending moment distributions computed at the critical condition, together with the theoretical distributions referring to $k_h = k_c$ and $k_h = k_{TF}$, where $k_c = 0.22 (= k_{GF})$ and $k_{TF} = 0.30$. At the onset of critical condition, the system still preserves some reserve of strength due to the fact that active limit conditions are not completely attained in the retained soil. Then, if the absolute acceleration of the system can increase beyond the critical value, as in the case of rotating systems (see *e.g.*, Conti and Caputo, 2019), contact pressures can further evolve, until the next local plastic mechanism is activated. And indeed, theoretical predictions for $k_h = k_{TF}$ do provide, in this case, a good estimate of maximum internal forces in the structural elements.

A final comparison between numerical results and theoretical predictions is presented in Figure 15 showing, for all layouts, the evolution of the normalised maximum bending moment, $M_{max}/\gamma H^3$, and axial force, $T_a/\gamma H^2$, as a function of k_h. In addition to the pseudo-static results, Figure 15 displays the

maximum internal forces computed in the dynamic analyses, as a function of the corresponding maximum free-field surface acceleration. For cases 1, 2 and 3, further dynamic analyses were carried out by scaling the applied inputs to lower values of the maximum acceleration, in order to investigate the response of the anchor-wall system under lower-intensity seismic excitations. Moreover, to explore the possible influence of the soil-wall relative stiffness on the numerical results, two further set of pseudo-static analyses were carried out for cases 1 and 2, in which the soil shear modulus was reduced by two-thirds (triangles in Figure 15a, b, e, f) and the bending stiffness of the wall was approximately doubled, to match that of an AZ48 profile (squares in Figure 15a, b, e, f).

As anticipated, for $k_h < k_c$, LE predictions tend to over-estimate the maximum bending moment and to under-estimate the anchor force. Instead, the maximum internal forces are well predicted by the proposed method, using either the actual critical acceleration, $k_h = k_c$, if the critical mechanism is local (cases 1 and 4 in Figure 15), or, in the case of global failure (cases 2 and 3 in Figure 15), the smaller value of yield acceleration computed for the two local plastic mechanisms, $k_h = \min(k_{AF}, k_{TF})$. Moreover, the relative soil-wall stiffness seems not to affect the numerical pseudo-static results, in terms of both critical acceleration and internal forces, similarly to what observed by Conti *et al.* (2014) for embedded cantilevered walls. This result is independent of the particular plastic mechanism activated within the soil-wall-anchor system.

The pseudo-static results shown in Figure 15 are in very good agreement with those provided by the dynamic analyses, thus indicating that possible phase-shifts or amplifications of soil accelerations do not affect significantly the overall behaviour of these systems and, therefore, even a simple pseudo-static approach can provide a satisfactory description of their response to seismic actions. Moreover, the computed pseudo-static internal forces provide a very good estimate of the maximum values that the structural members can ever experience under a real earthquake.

A more in-depth comparison between LE predictions and numerical dynamic analyses is provided in Figures 16 and 17, referring to case 1 subjected to the Friuli earthquake. Figure 16 shows the time histories of: (a) the free-field surface acceleration and the horizontal acceleration and displacement

computed at the top of the right wall; (b) the bending moment computed in the right wall at a depth of z = 7 m, where the internal forces reach their maximum during the applied earthquake. The pseudo-static LE values of a_c and $M_{max}(a_c)$ are also reported in the figure. Moreover, for the time instant corresponding to which the bending moment in the right wall attains its maximum value (t = 6.1 s), Figure 17 shows the distribution of: (a) soil contact pressures and horizontal displacements of the main wall; (b) bending moments and (c) free-field soil accelerations. During the strong motion stage (approximately between 3 s and 8 s), the bending moment increases due to the applied soil inertia forces and the wall progressively rotates (Figure 16). The peak internal forces are attained in time instants when the wall is accumulating permanent displacements, *i.e.*, when the accelerations of the soil-wall system differ from those in the free-field. In these time instants, the strength of the anchor system is locally attained and the distributions of both soil-wall contact pressures and bending moment are in excellent agreement with the LE critical ones (Figure 17a, b).

5. CONCLUSIONS

This work focused on the seismic design of ASSP retaining walls. The main conclusions and results can be summarised in the following points:

- Potential dissipative plastic mechanisms for ASSP walls correspond either to the local attainment of the soil shear strength in the supporting soil (toe failure) and around the anchor (anchor failure), or in the activation of a log-spiral global failure surface (global failure).
- For these mechanisms, a new pseudo-static LE method was proposed to compute the corresponding values of acceleration and, in turn, the critical acceleration of the system. The proposed method allows also to compute the internal forces in the structural members (bending moment in the main wall and axial force in the tie rods) and the anchor capacity.
- Based on a theoretical parametric study, carried out under pseudo-static conditions, it was concluded that for typical layouts of ASSP walls the most likely failure mechanisms are local anchor failure and global failure.

- The predictive capabilities of the proposed method were assessed against existing dynamic centrifuge data and the results of original numerical pseudo-static and dynamic FD analyses. The predicted values of the critical accelerations and of the maximum internal forces are in very good agreement with the numerical results. This point is of major relevance when dealing with performance-based seismic design of ASSP walls (as recommended in modern codes), where dissipative plastic mechanisms are allowed to develop within the soil-wall-anchor system.
- Dynamic FD analyses indicate that the structural internal forces cannot increase further once the soil shear strength is locally fully mobilised by either toe or anchor failure. This condition imposes a physical upper-bound to the maximum values that the internal forces can ever attain during an earthquake. As a result, a safe and efficient seismic design of the structural members should be carried out using $k_h = \min(k_{AF}, k_{TF})$ as the reference pseudo-static coefficient.

The data discussed in the paper refer only to ASSP walls in dry sand; further research is required to include possible relevant effects arising from the presence of water in the backfill and in front of the wall.

Data Availability Statement

Some or all data, models, or code that support the findings of this study are available from the corresponding author upon reasonable request.

Acknowledgements

Part of this work was carried out while the first Author was supported by a research grant from ArcelorMittal.

APPENDIX

462 The static design of ASSP walls depends on 13 physical variables: 7 variables describing the system
463 layout (H, D, b, L, H_A, b_A, c), 3 variables describing the soil mechanical properties (ϕ', δ, γ) and 3
464 variables describing the structural response of the system (M_{max}, T_a, T_{lim}).
465 Using the standard Free-End Method for the static design of the main wall and assuming $\delta = 1/3\phi'$,
466 application of dimensional analysis leads to the following formulation for the problem at hand:

467 $$D/H = G_1(b/H, \phi') \quad \text{(A1)}$$

468 $$M_{max}/(\gamma H^3) = G_2(b/H, \phi') \quad \text{(A2)}$$

469 $$T_a/(\gamma H^2) = G_3(b/H, \phi') \quad \text{(A3)}$$

470 Similarly, assuming a conventional triangular distribution of the passive and active soil pressures in
471 front of and behind the anchor plate, and $\delta = 0°$ (Ebeling & Morrison 1993), the following
472 dimensionless equation for the computation of the anchor capacity is obtained:

473 $$T_{lim}/(\gamma H_A^2) = G_4(\phi') \quad \text{(A4)}$$

474 which, introducing a safety factor $SF_A = T_{lim}/T_a$, reduces to:

475 $$H_A/H = G_5(b/H, \phi', SF_A) \quad \text{(A5)}$$

476 A minimum length of the tie rods (L_{min}) must be defined in order to avoid overlapping of the active
477 and passive soil wedges possibly developing behind the main wall and in front of the anchor plate,
478 respectively. Thus, using conventionally the Rankine theory (Rankine, 1857) and introducing a safety
479 factor $SF_L = L/L_{min}$, the choice of the tie rods length is defined by the following dimensionless
480 equation:

481 $$L/H = G_6(b/H, \phi', SF_A, SF_L) \quad \text{(A6)}$$

482 Based on these considerations, a conventional static design implies that the geometry of an ASSP
483 wall is defined by three dimensionless ratios (D/H, H_A/H and L/H), which depend upon the two
484 dimensionless parameters ϕ' and b/H, through the safety factors SF_A and SF_L. Due to the assumptions
485 on the earth pressure distributions on the anchor wall, parameters c and b_A are not considered in the

static design, even though they do play a role in the determination of both the actual capacity of the anchor and the critical acceleration of the system.

References

Anderson, D.G., Martin, G.R., Lam, I., and Wang, J.N. (2009). "Seismic analysis and design of retaining walls, buried structures, slopes, and embankments." NCHRP Rep. 611, Transportation Research Board, Washington, D.C.

Becci B. & Carni M., (2014),"Pseudo-Static Analysis Of Flexible Retaining Structures Including Seismic Thrust Dependency On Wall Deformation", Proc. Conf. ISSMGE - TC207 "Soil-Structure Interaction. Underground Structures and Retaining walls, Saint Petersburg, June 16-18, pp. 277-284.

Callisto, L. (2014). "Capacity design of embedded retaining structures". *Géotechnique*, 64(3), 204–214.

Callisto L., Del Brocco I. (2015). "Intrinsic seismic protection of cantilevered and anchored retaining structures". In Proceedings of the SECED Conference on Earthquake Risk and Engineering towards a Resilient World, Cambridge UK.

Caputo G., Conti, R., Viggiani, G.M.B., Prüm, C. (2019). "Theoretical framework for the seismic design of anchored steel sheet pile walls". Proceedings of the 'VII International Conference on Earthquake Geotechnical Engineering' – Rome, Italy.

Conte, E., Troncone, A., Vena, M. (2017). "A method for the design of embedded cantilever retaining walls under static and seismic loading". *Géotechnique*, 67(12), 1081–1089.

Conti, R., Viggiani, G.M.B., Cavallo, S. (2013). "A two-rigid block model for sliding gravity retaining walls". *Soil Dyn. Earthquake Eng*. 55, 33–43.

Conti, R., Viggiani, G.M.B, Burali d'Arezzo, F. (2014). "Some remarks on the seismic behaviour of embedded cantilevered retaining walls". *Géotechnique*, 64(1), 40-50.

512 Conti, R., Caputo, G. (2018). “A numerical and theoretical study on the seismic behaviour of yielding
513 cantilever walls”. *Géotechnique*, 69(5), 377-390.
514 Ebeling. R.M., E.E. Morrison. Jr. (1993) "The seismic design of waterfront retaining structures." US
515 Army Corps of Engineers. Waterways Experiment Station, Technical Report ITL-92-11. 256p.
516 Elms D. A., G. R. Martin (1979). “Factors Involved in the Seismic Design of Bridge Abutments.”
517 Proceedings, Workshop on Seismic Problems Related to Bridges, Applied Technology Council,
518 San Diego, Calif.
519 Fusco A., Viggiani, G.M.B., Madabhushi G., Caputo G., Conti, R., Prüm, C. (2019). “Physical
520 modelling of anchored steel sheet pile walls under seismic actions”. Proceedings of the ‘VII
521 International Conference on Earthquake Geotechnical Engineering’ – Rome, Italy.
522 Gazetas, G., Garini E., Zafeirakos A. (2016). “Seismic analysis of tall anchored sheet-pile walls”,
523 *Soil Dyn. Earthquake Eng*, 91, 209-221.
524 Japan Port and Harbour Association (JPHA) (1989). "Technical Standards for Port and Harbour
525 Facilities in Japan," English version (1991) by the Overseas Coastal Area Development Institute
526 of Japan, 438p.
527 Kloukinas, P., Scotto di Santolo, A., Penna, A., Dietz, M., Evangelista, A., Simonelli, A.L., Taylor,
528 C., Mylonakis, G. (2015). “Investigation of seismic response of cantilever retaining walls: Limit
529 analysis vs shaking table testing”. *Soil Dyn. Earth. Eng*., 77, 432-445.
530 Lai, S. (1998). “Rigid and flexible retaining walls during Kobe earthquake”. Proc. 4th International
531 Conference on Case Histories in Geotechnical Engineering, St. Louis, 108–127.
532 Lancellotta, R. (2007). “Lower-bound approach for seismic passive earth resistance”. *Géotechnique*,
533 57(3), 319–321..
534 Littlejohn, G. S.. (1972). "Anchored Diaphragm Walls in Sand—Anchor Design," *Ground*
535 *Engineering*, 5(1), 12-17
536 Madabhushi S. P. G.; Zeng X. (2007). “Simulating Seismic Response of Cantilever Retaining Walls”.
537 *J. Geotech. and Geoenvir. Engng.*, 133(5), 539–549.

Mononobe, N. & Matsuo, H. (1929). “On the determination of earth pressure during earthquakes”. Proceedings of the world engineering congress, Tokyo, 9, 177-185.

NCHRP National Cooperative Highway Research Program. (2008). “Seismic analysis and design of retaining walls, buried structures, slopes and embankments”. Technical Report 611, Transportation Research Board, Washington DC.

Neelakantan, G., Budhu, M., and Richards, R., Jr. (1990). "Mechanics and performance of a tied-back wall under seismic loads." *Earthquake Engrg. and Struct. Dynamics*, 19(3), 315-331.

Neelakantan G.; Budhu M.; Richards R. (1992). “Balanced seismic design of anchored retaining walls”. *Journal of Geotechnical Engineering*, 118(6), 873–888.

Newmark N. M. (1965). “Effects of earthquakes on dams and embankments”. *Géotechnique*, 15(2), 139–160.

Okabe, S. (1924). “General theory on earth pressure and seismic stability of retaining wall and dam”. *J. Japan. Civ. Engng Soc*. 10(5), 1277–1323.

PIANC (2001). “Seismic design guidelines for port structures”. Working Group no. 34 of the Maritime Navigation Commission, p.474. Rotterdam, the Netherlands: International Navigation Association, Balkema.

Rankine, W.J.M. (1857). “On the stability of loose earth”. *Philosophical Transactions of the Royal Society of London*, 147, 9 – 27.

Richards R., Elms D. (1979). “Seismic behavior of gravity retaining walls”. *J Geotech Eng Div*, 105(4), 449–64.

Zeng X., Steedman R. S. (1993). “On the behaviour of quay walls in earthquakes”. *Geotechnique*, 43(3), 417–431.

Table 1. Problem layouts: dimensionless numbers investigated and yield accelerations.

	dimensionless numbers			yield/critical accelerations [g]			
case	b_A/H_A	L/H	D/H	a_{TF}	a_{AF}	a_{GF}	a_c
1	1/3	2.1	0.4	-	0.13	0.19	0.13
2	2/3	2.1	0.4	0.3	-	0.22	0.22
3	1/3	1.5	0.4	-	0.13	0.08	0.08
4	1/3	2.1	0.5	-	0.15	0.21	0.15

Table 2. Ground motion parameters of the input earthquakes.

#	Earthquake	*PGA* [g]	*PGV* [m/s]	*PGD* [m]	f_d [Hz]	f_m [Hz]	I_a [m/s]	$T_{5\text{-}95}$ [s]
1	Kobe - Japan (1995)	0.329	0.281	0.116	0.60	3.44	1.65	18.6
2	Imperial Valley - USA (1979)	0.330	0.307	0.162	1.90	3.81	1.21	10.3
3	Hollister - Usa (1961)	0.194	0.120	0.044	2.36	2.13	0.25	9.2
4	Chi Chi - Taiwan (1999)	0.214	0.198	0.180	1.12	3.24	0.26	9.4
5	Friuli - Italy (1976)	0.324	0.221	0.042	2.00	3.21	0.76	4.8
6	Kocaeli - Turkey (1999)	0.329	0.281	0.116	0.60	3.44	1.65	18.6

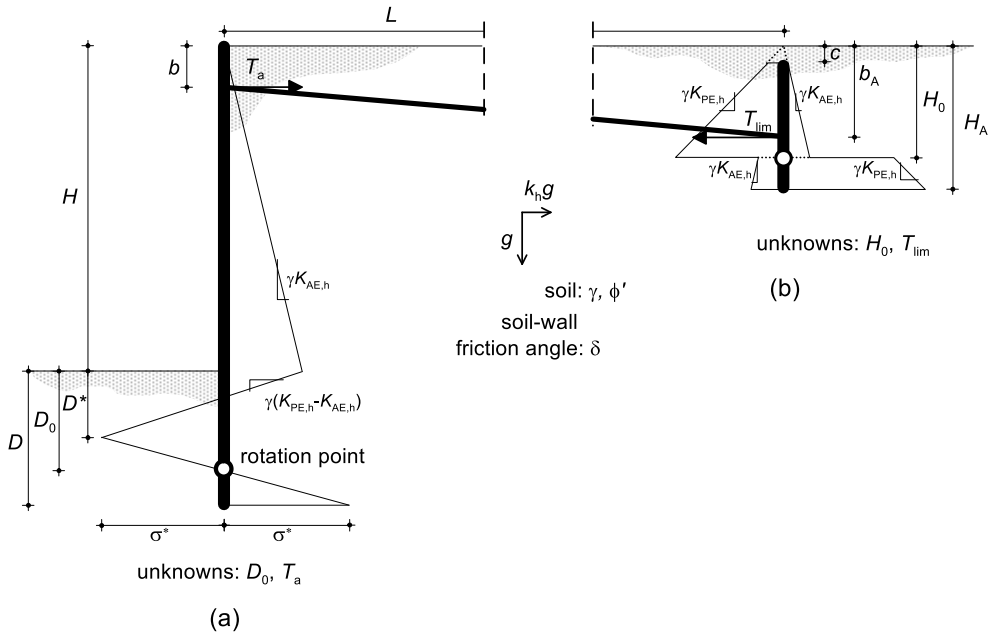

Figure 1. Typical layout of an ASSP wall and earth pressure distributions assumed in the proposed pseudo-static limit equilibrium method: (a) main wall and (b) anchor plate.

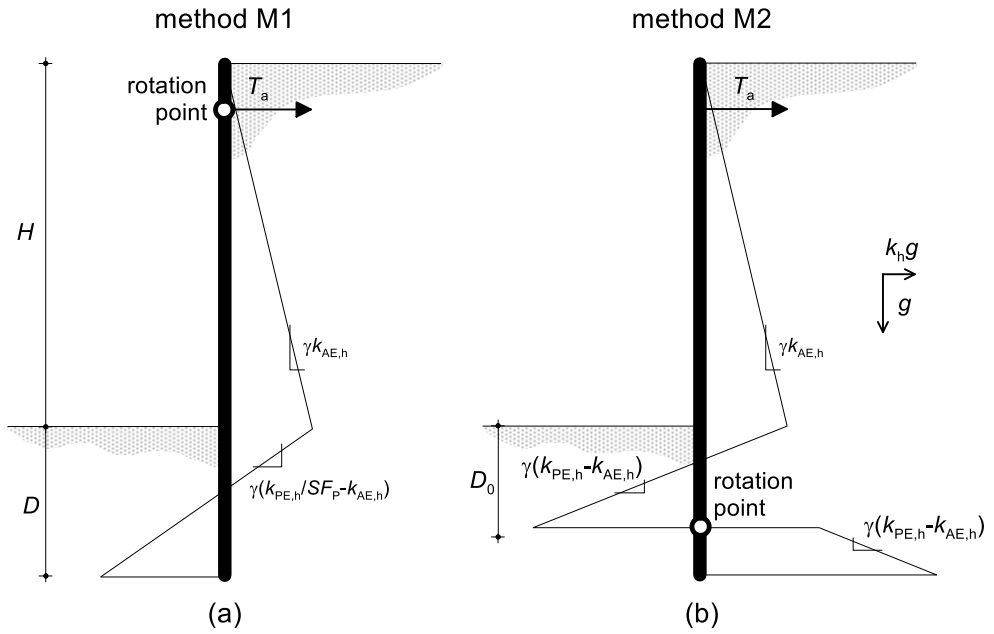

Figure 2. Pseudo-static net pressure distributions according to: (a) method M1 (Neelakantan *et al.* 1992); and (b) method M2 (Zeng & Steedman, 1993).

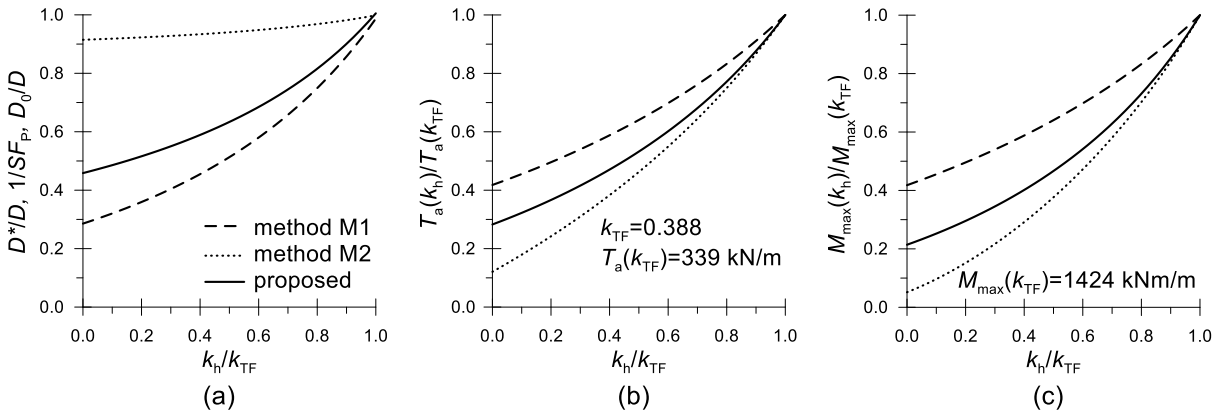

Figure 3. Comparison between pseudo-static LE methods in terms of: (a) mobilised passive strength in front of the wall; (b) normalised axial force in the tie rod, $T_a(k_h)/T_a(k_{TF})$; and (c) normalised maximum bending moment in the wall, $M_{max}(k_h)/M_{max}(k_{TF})$, as a function of k_h/k_{TF} ($\gamma = 20$ kN/m^3, $\phi' = 35°$, $\delta = \phi'/3$, $D/H = 0.5$, $b/H = 0.1$).

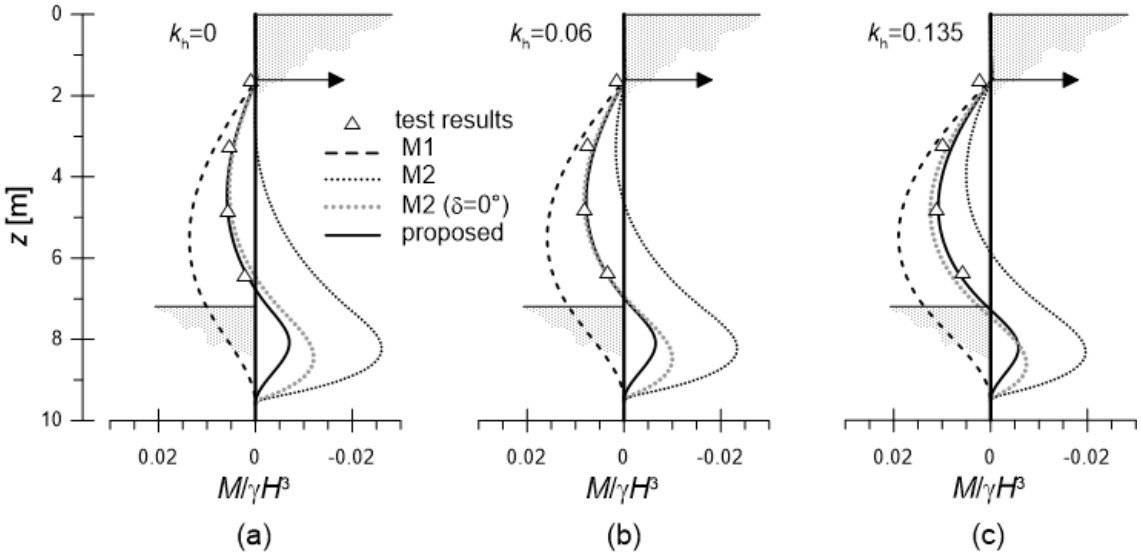

Figure 4. Dynamic centrifuge test results published by Zeng & Steedman (1993). Comparison between experimental data and theoretical LE predictions of bending moments for: (a) $k_h = 0$ (static); (b) $k_h = 0.06\ g$; (c) $k_h = 0.135\ g$.

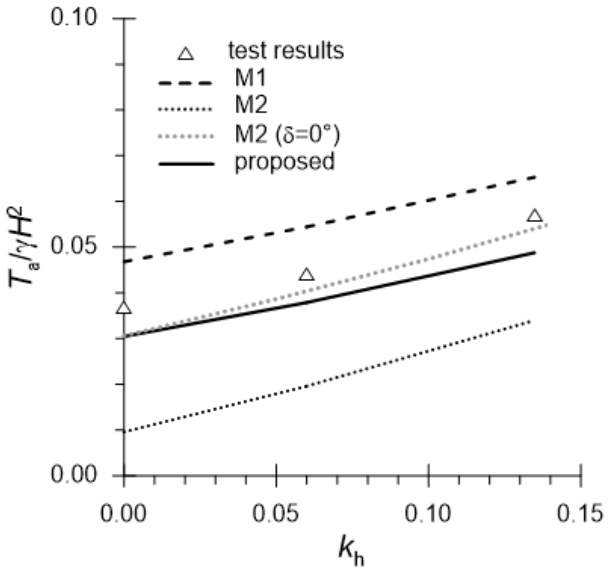

Figure 5. Dynamic centrifuge test results published by Zeng & Steedman (1993). Comparison between experimental data and theoretical LE predictions of the axial force in the tie rod.

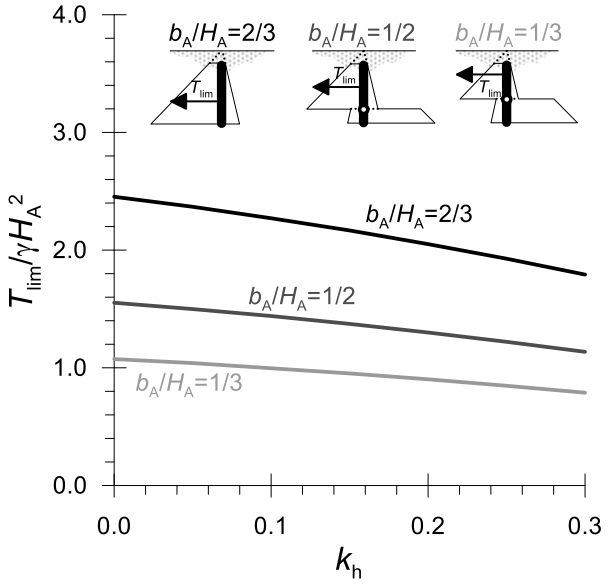

Figure 6. Proposed LE method: normalised anchor resistance $T_{lim}/\gamma H_A^2$, as a function of k_h, for different anchor layouts (c = 0, H_A = 3.2 m, γ = 20 kN/m^3, ϕ' = 35°, $\delta = \phi'/3$).

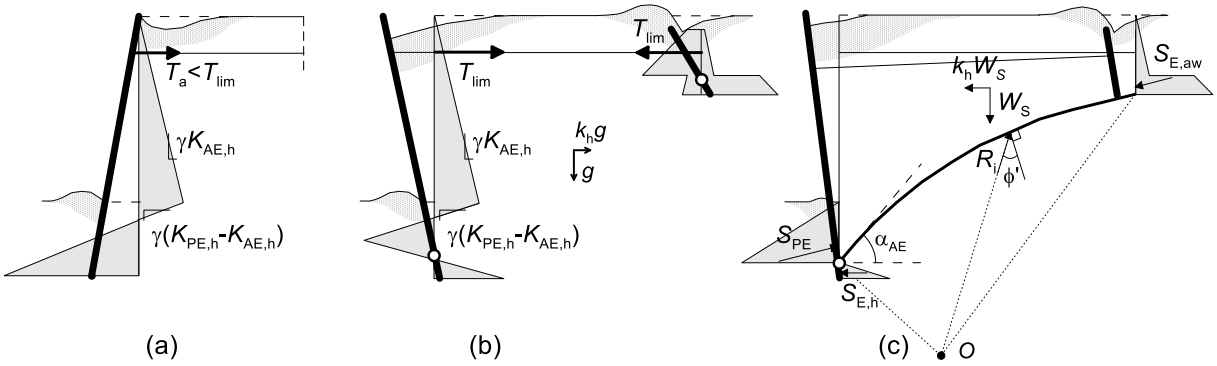

Figure 7. Potential plastic mechanisms for ASSP walls. Schematic deformed shape and LE earth pressure distributions at the onset of the yielding condition: (a) toe failure; (b) anchor failure and (c) global failure.

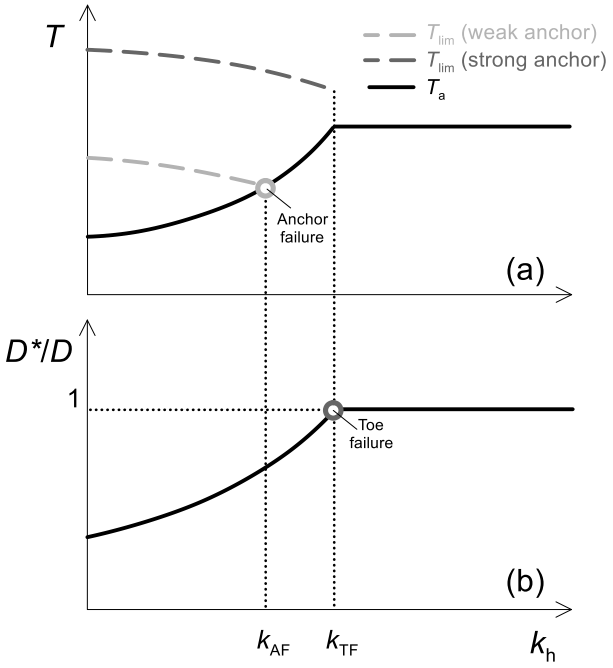

Figure 8. Schematic representation of: (a) the anchor force required for the stability of the retaining wall, T_a, and the anchor resistance, T_{lim}; and (b) the ratio D^*/D, as a function of k_h, for different anchor layouts (strong and weak anchor).

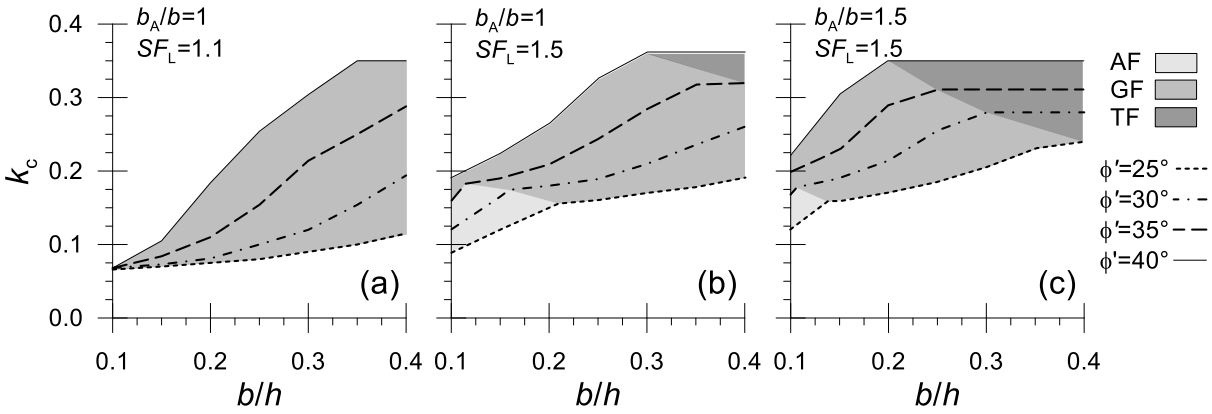

Figure 9. Theoretical parametric study: critical acceleration of the examined ASSP wall layouts: (a) b_A/b = 1 and SF_L = 1.1; (b) b_A/b = 1 and SF_L = 1.5; (c) b_A/b =1.5 and SF_L = 1.5.

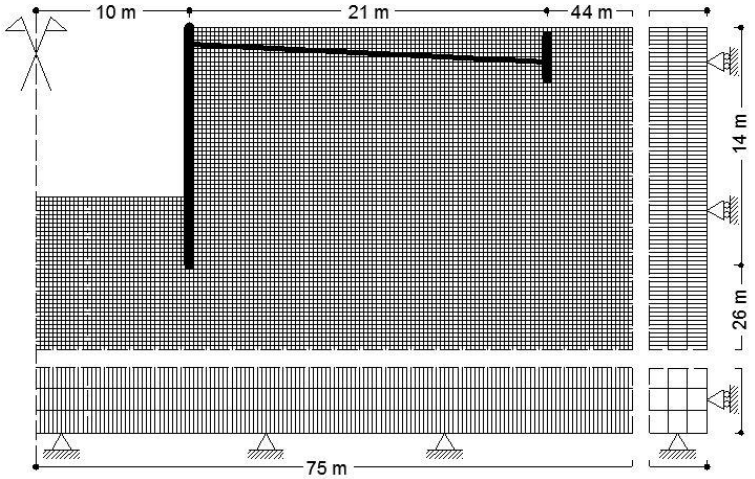

Figure 10. Detail of the finite difference grid adopted in the numerical analyses (case 2), together with the boundary constraints adopted for the static and the pseudo-static stages.

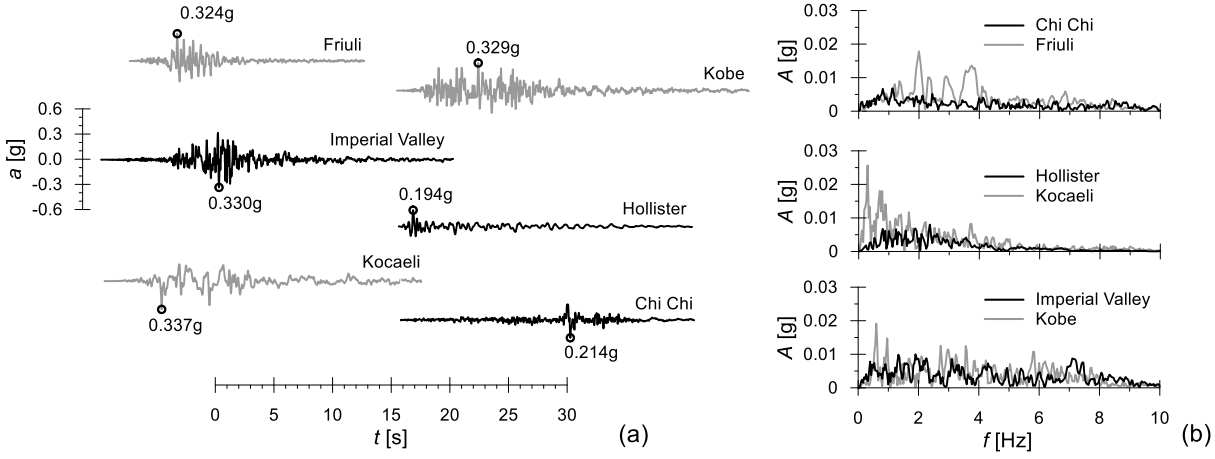

Figure 11. (a) Acceleration time histories and (b) Fourier amplitude spectra of the input earthquakes.

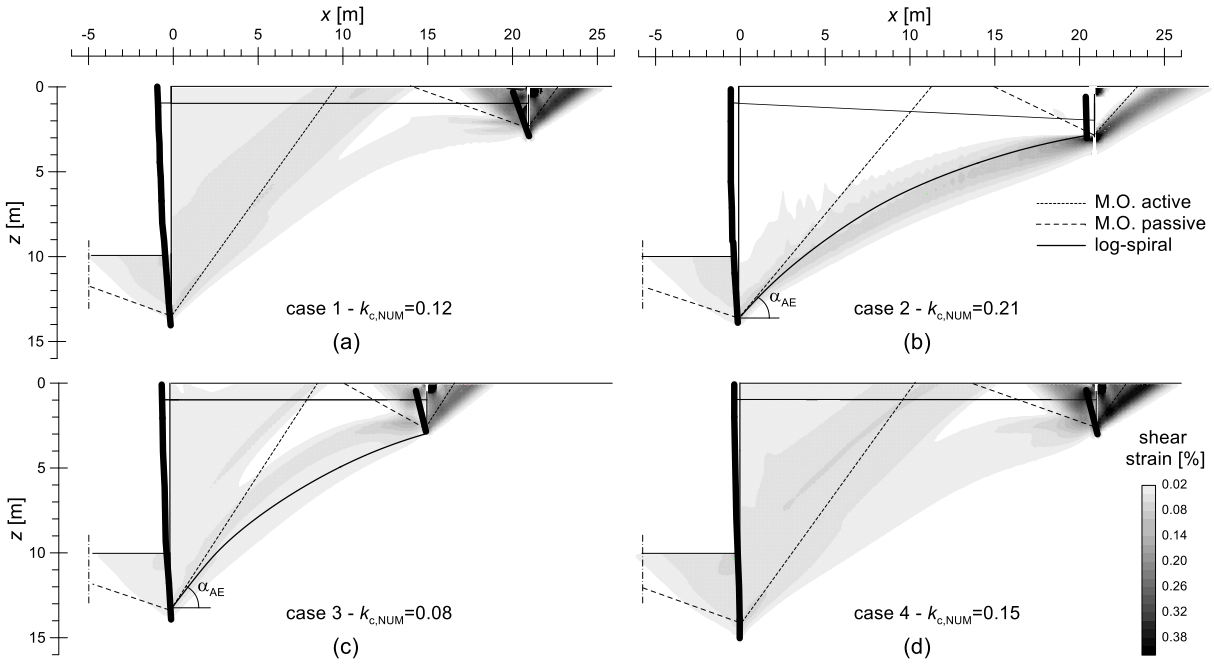

Figure 12. Numerical pseudo-static analyses: contours of shear strains at the critical condition and comparison with the theoretical LE predictions. (a) case 1, (b) case 2, (c) case 3, and (d) case 4.

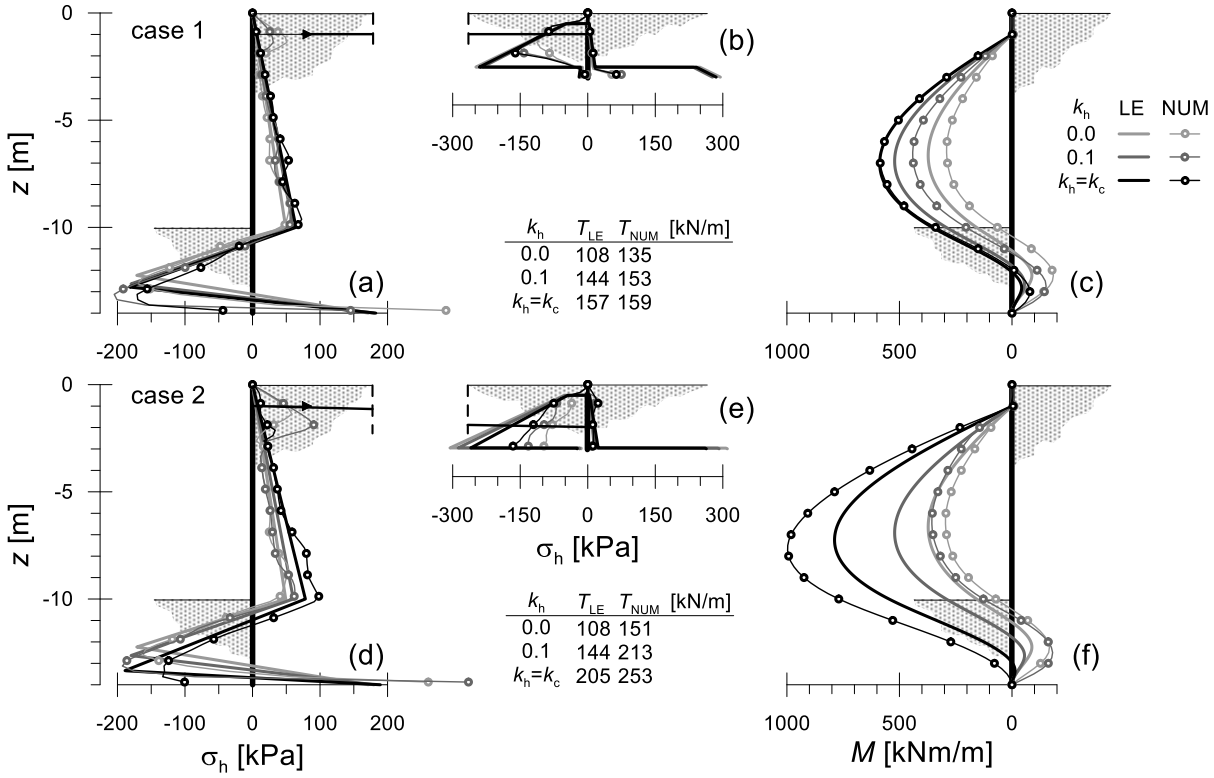

Figure 13. Comparison between pseudo-static numerical results and LE predictions for case 1 (anchor failure) and case 2 (global failure): (a, d) contact net pressures on the main wall; (b, e) contact pressures on the anchor plate; (c, f) bending moment distribution on the main wall. Data refer to three values of the pseudo-static coefficient, *i.e.*, k_h = 0, k_h = 0.1 and k_h = k_c.

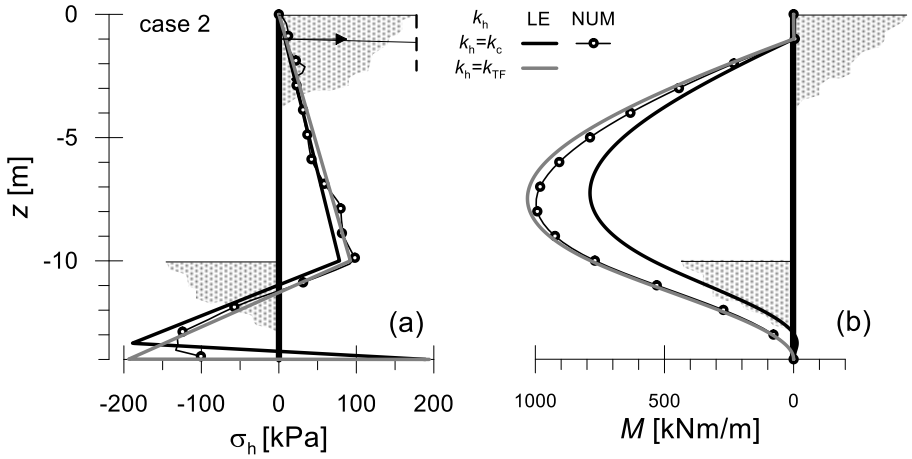

Figure 14. Case 2 (global plastic mechanism). Comparison between numerical pseudo-static results computed at the critical condition and theoretical predictions for $k_h = k_c$ and $k_h = k_{TF}$, in terms of (a) contact net pressure and (b) bending moment.

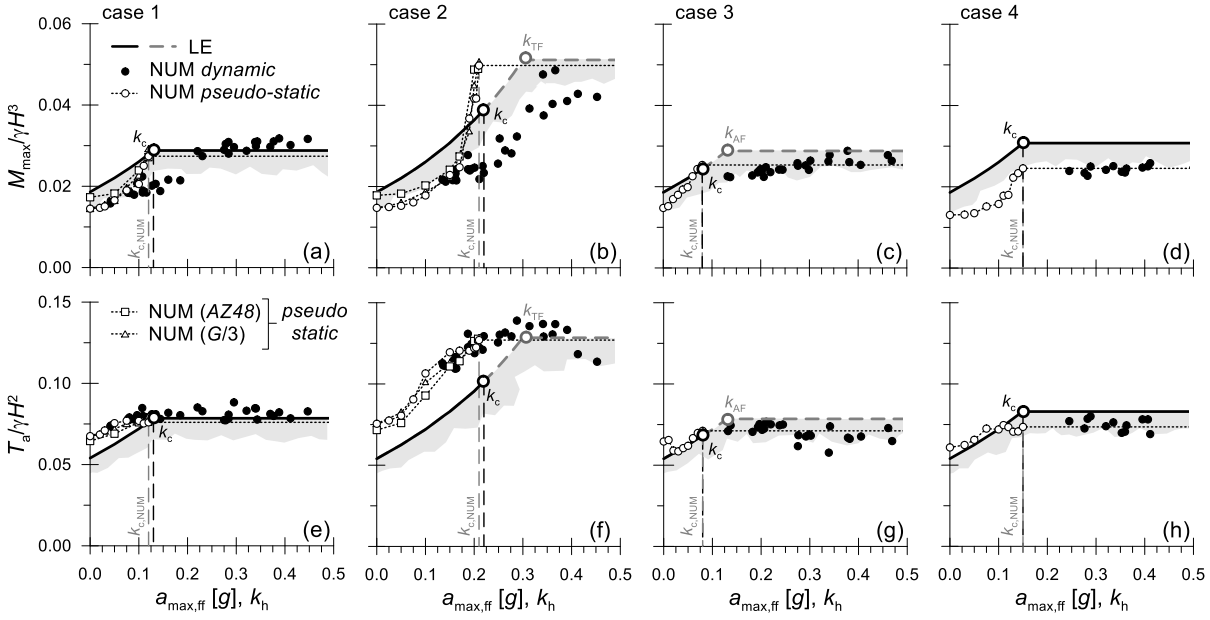

Figure 15. Comparison between numerical dynamic and pseudo-static analyses and LE predictions for all layouts, in terms of: (a, b, c, d) maximum bending moment, $M_{max}/\gamma H^3$ and (e, f, g, h) maximum anchor force, $T_a/\gamma H^2$. Dynamic values are plotted as a function of the maximum free-field acceleration, while pseudo-static values are given as a function of k_h.

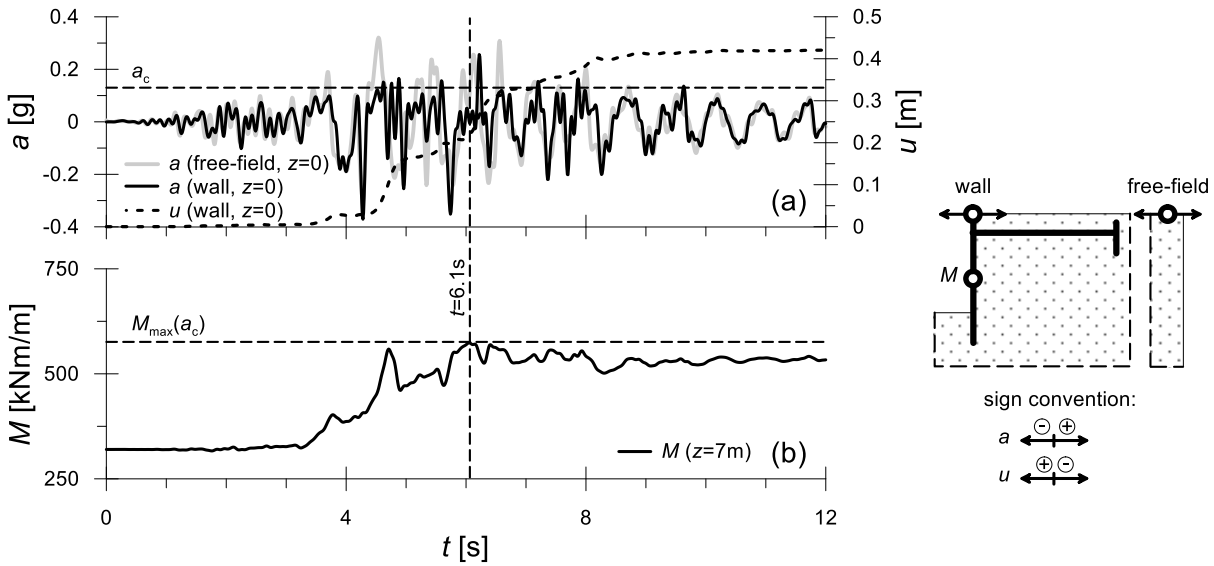

Figure 16. Dynamic numerical analyses (case 1, Friuli earthquake, right wall). Time histories of: (a) horizontal free-field surface acceleration and wall horizontal acceleration and displacement; (b) bending moment at z = 7 m.

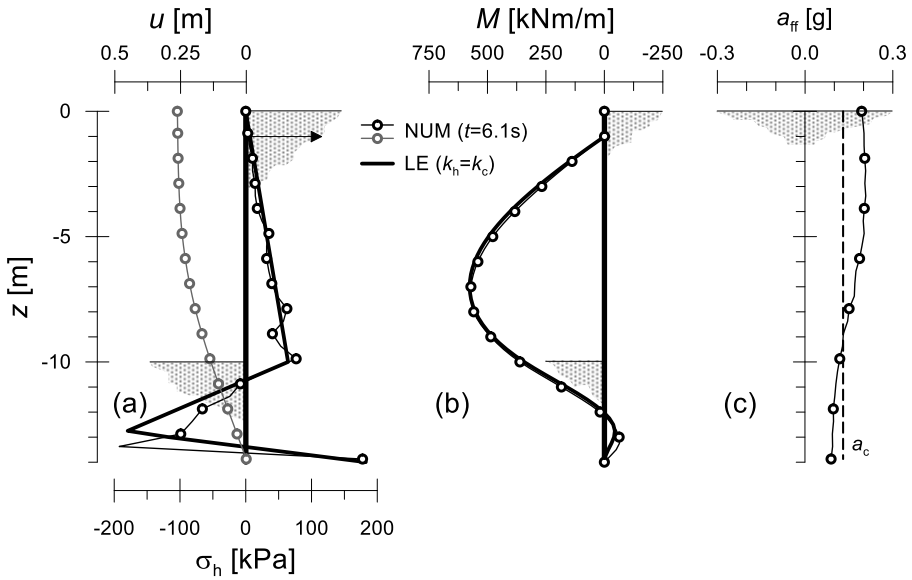

Figure 17. Dynamic numerical analyses (case 1, Friuli earthquake, right wall). Distributions (at t = 6.1 s) of: (a) contact net pressures and horizontal displacements of the wall; (b) bending moments and (c) free-field horizontal accelerations.

Figure 01

Click here to access/download;Figure;figure_01.tif

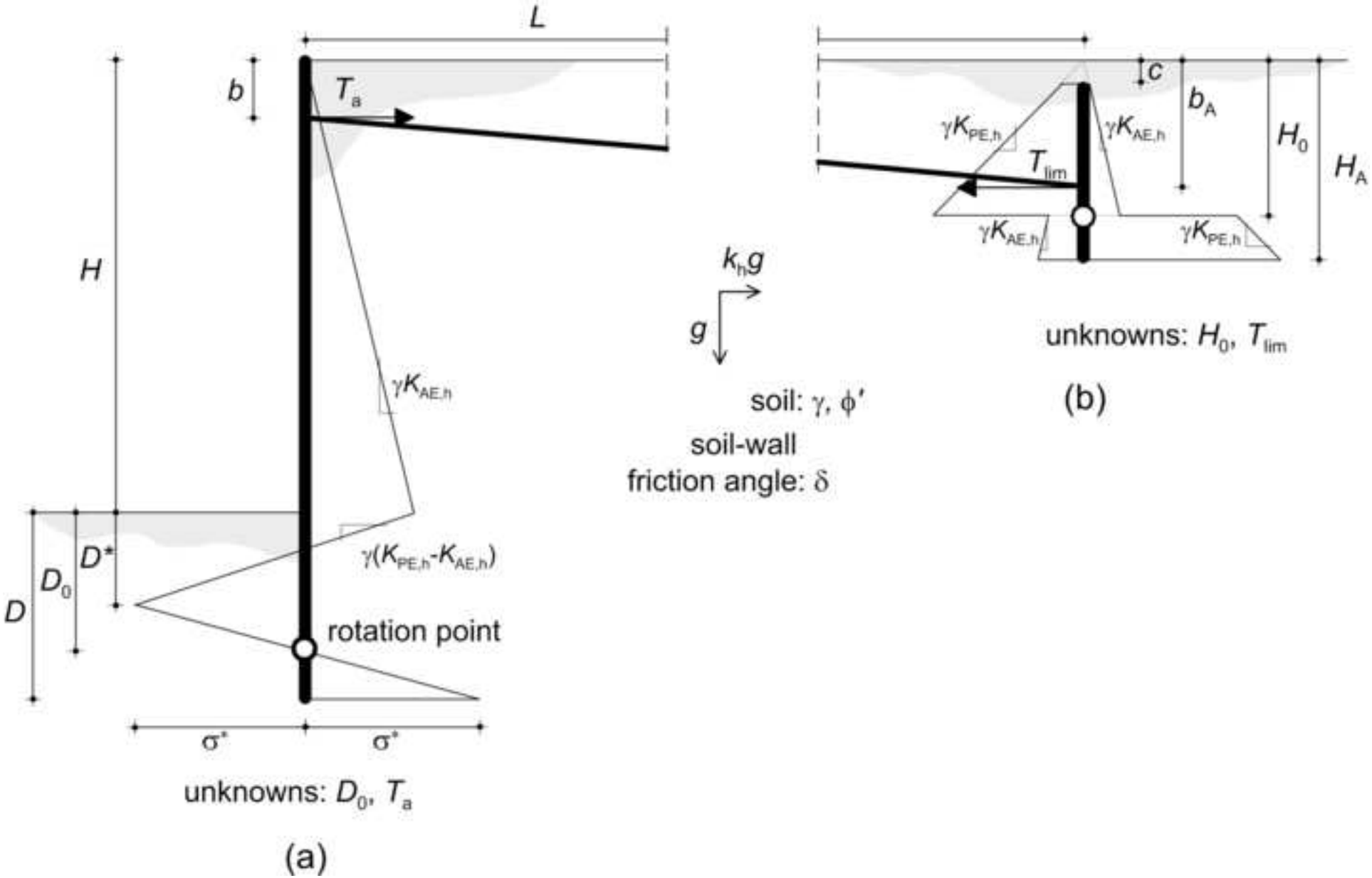

Figure 02

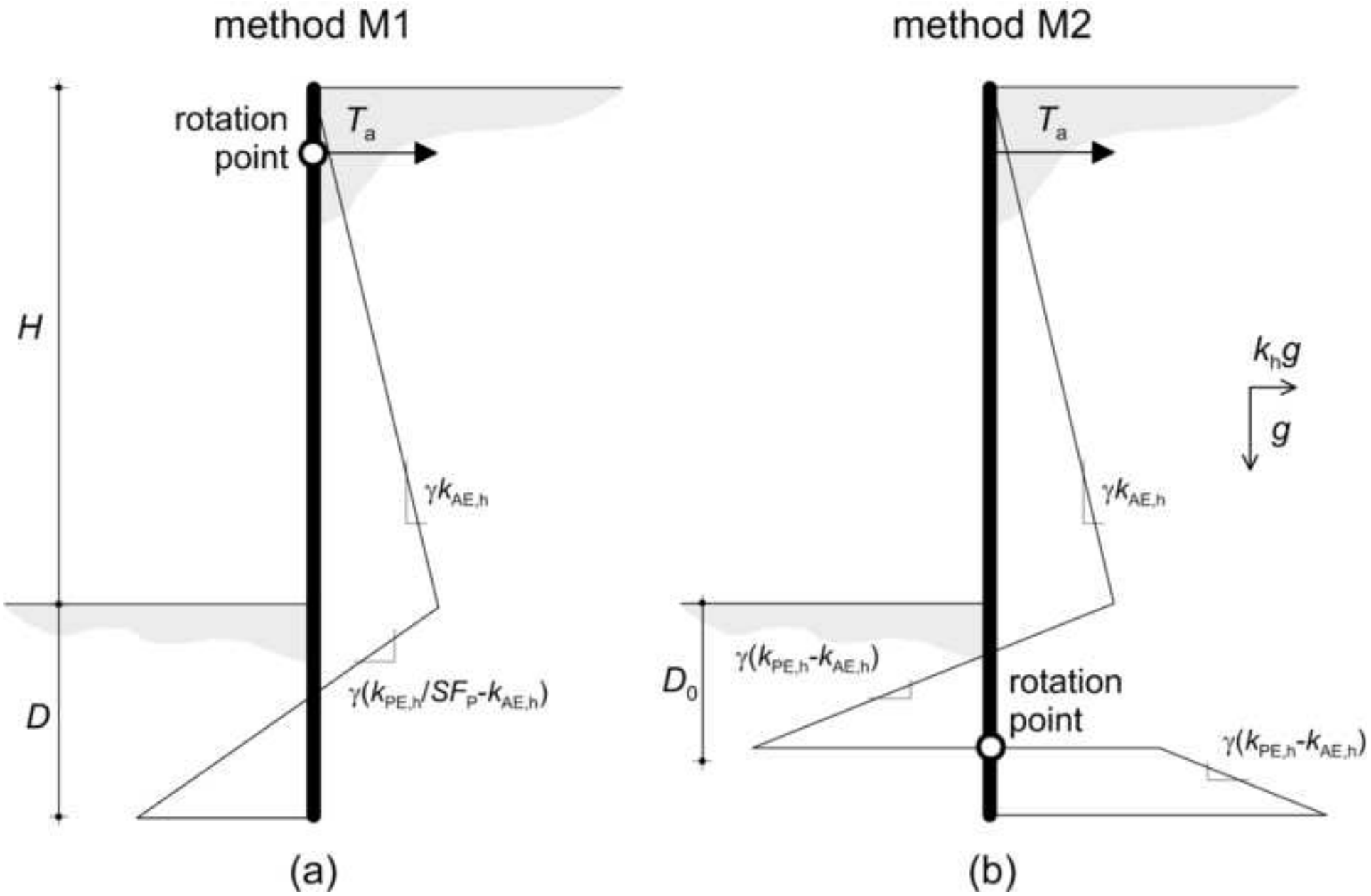

Figure 03

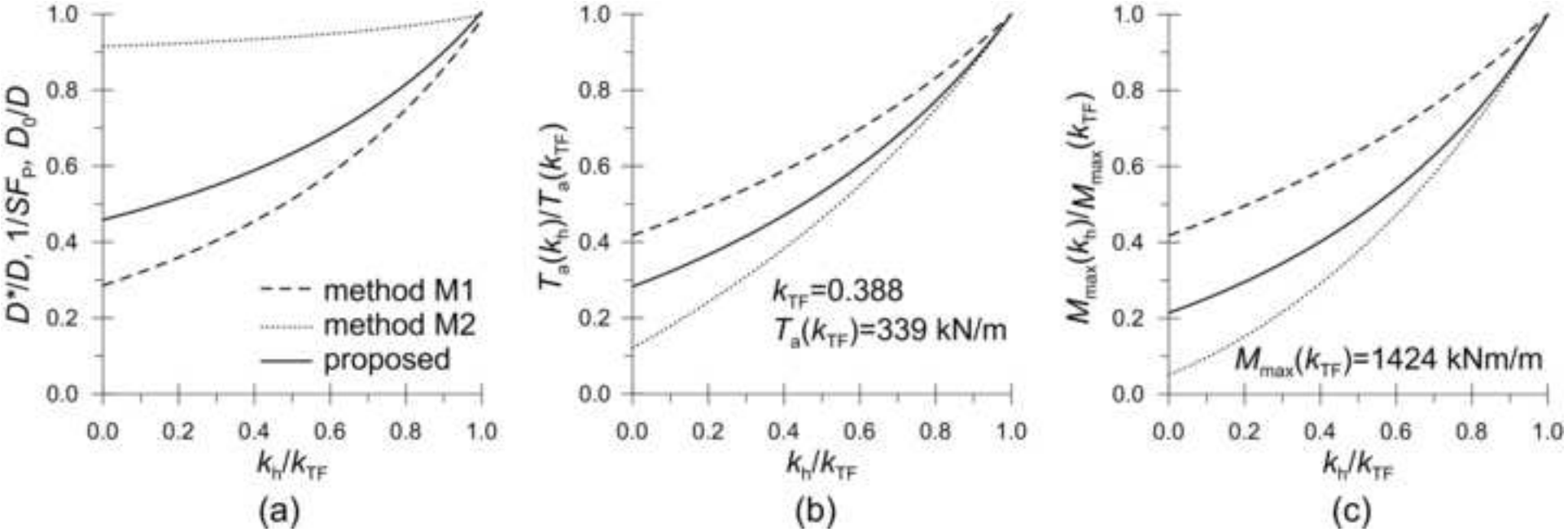

Figure 04

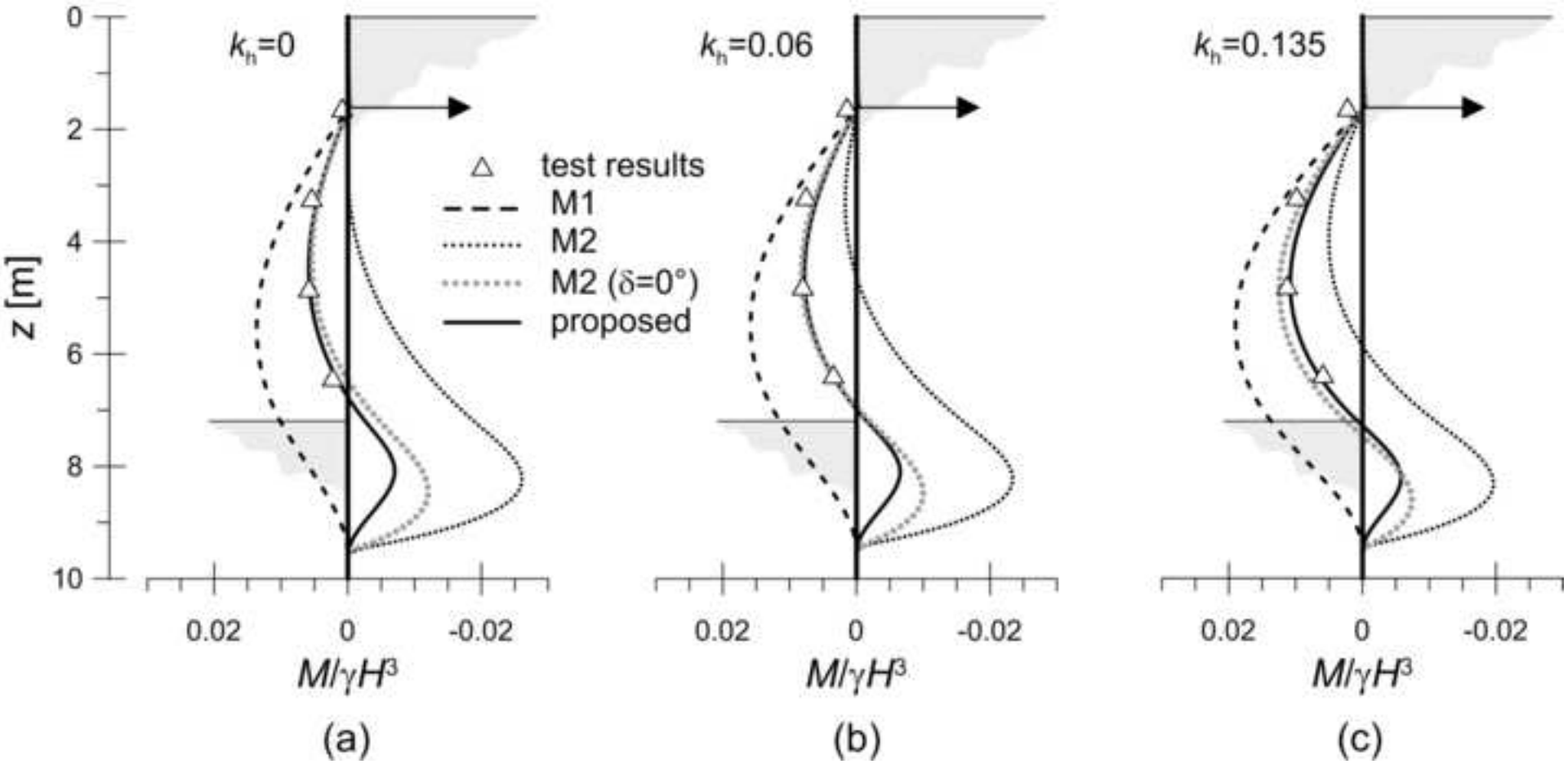

Figure 05

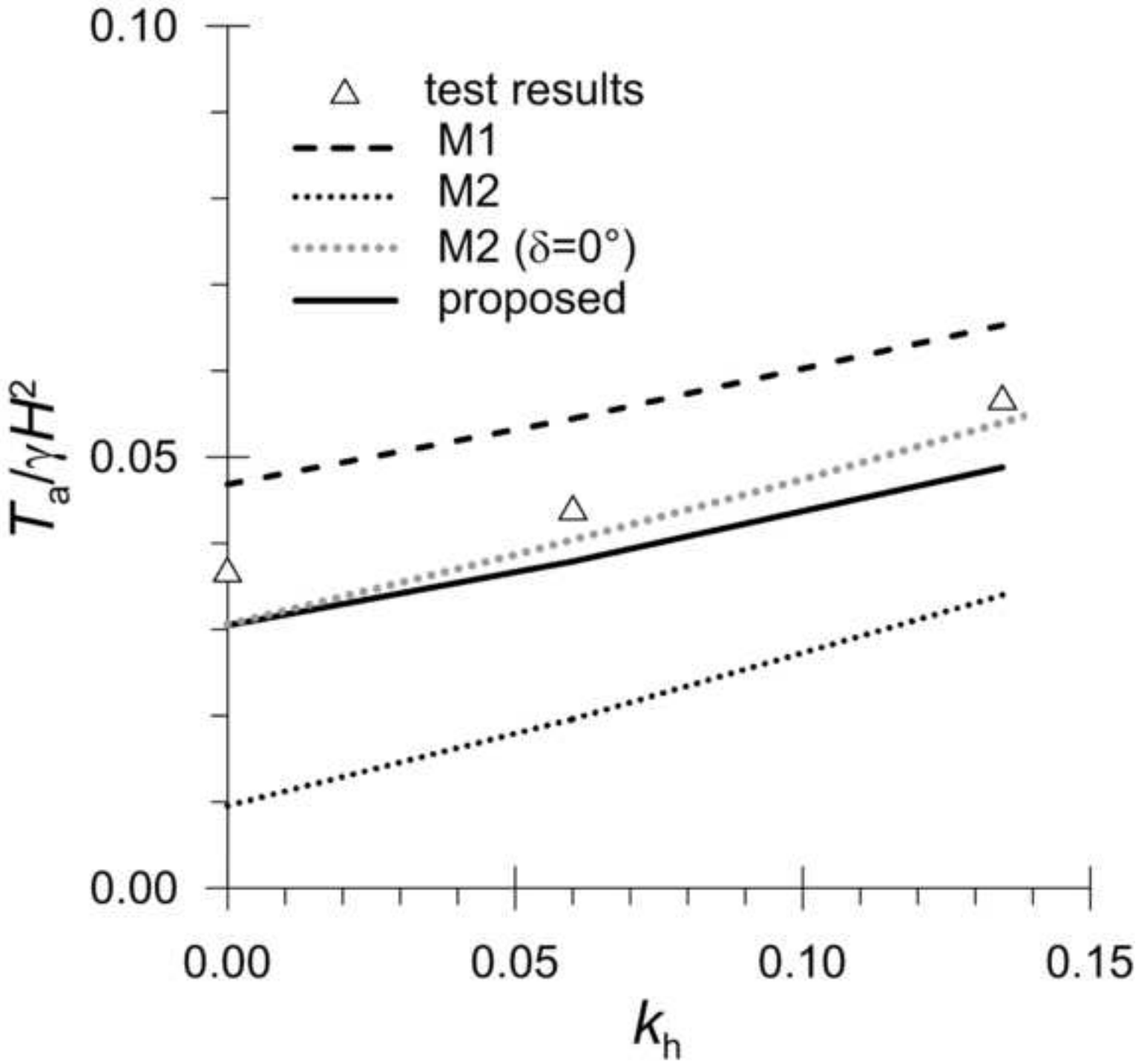

Figure 06

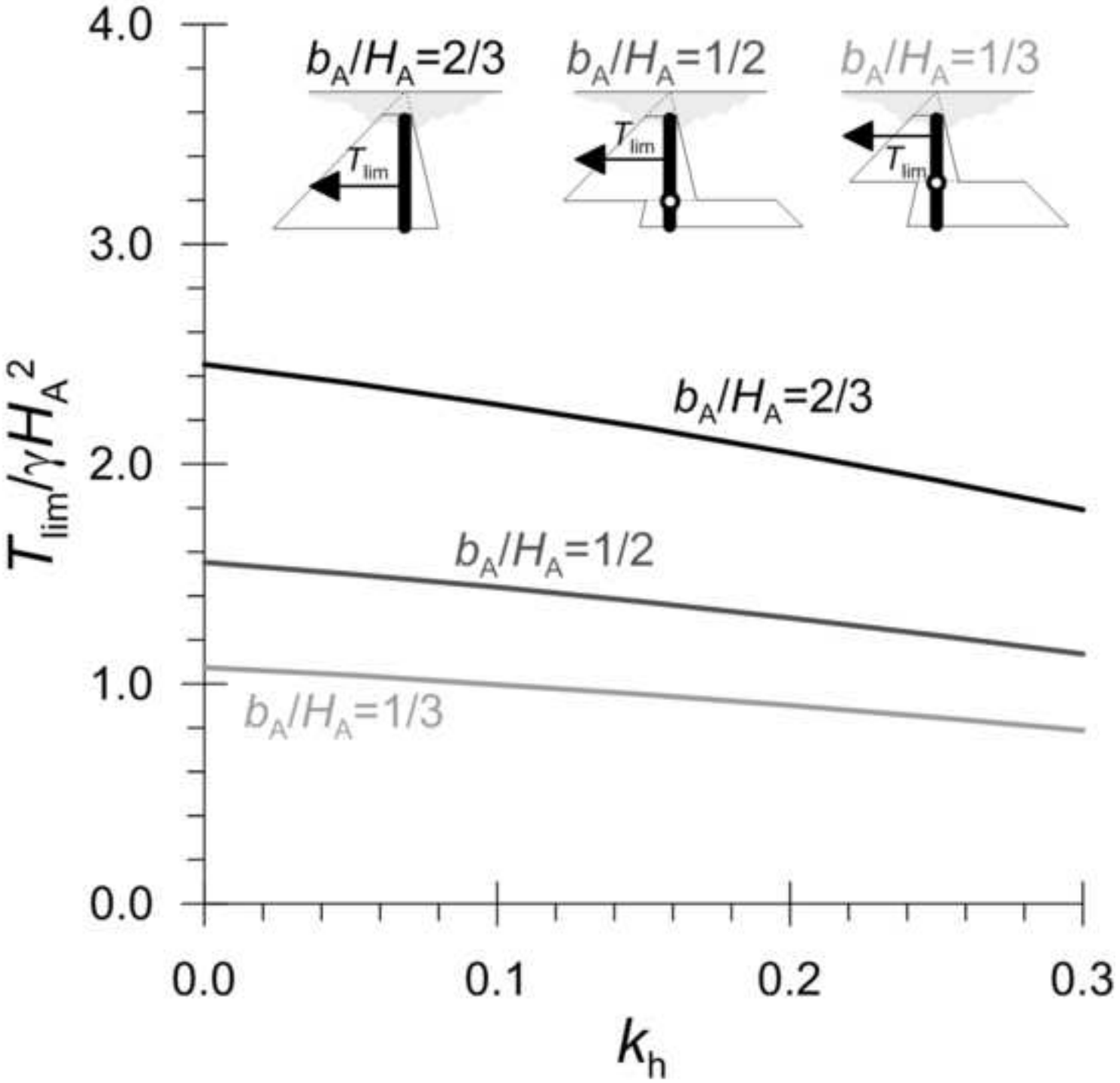

Figure 07

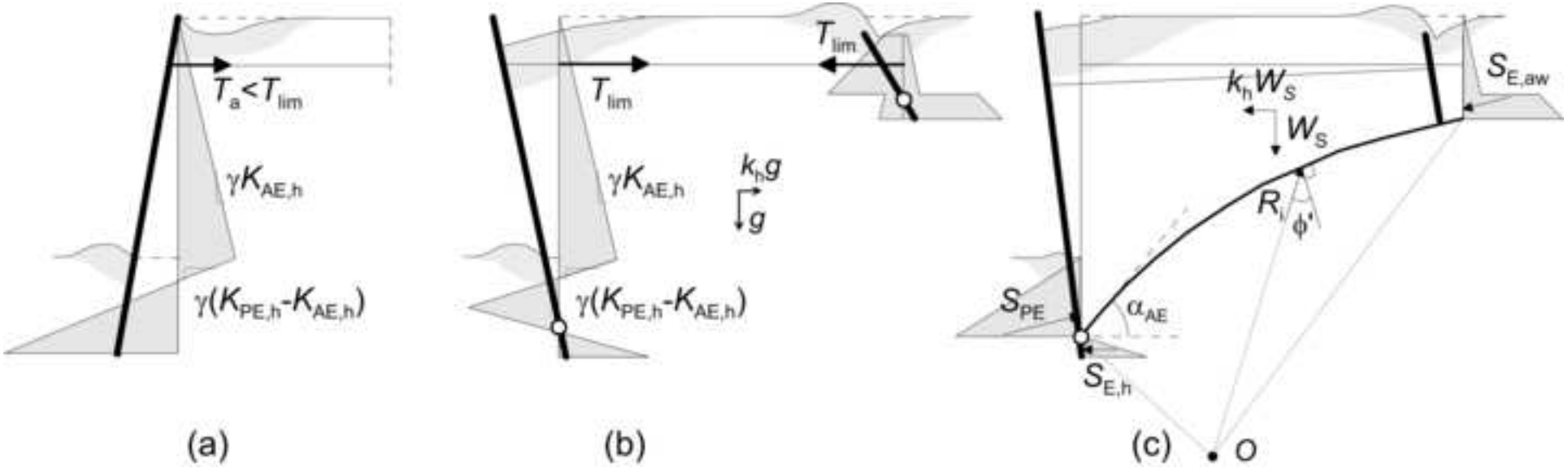

Figure 08

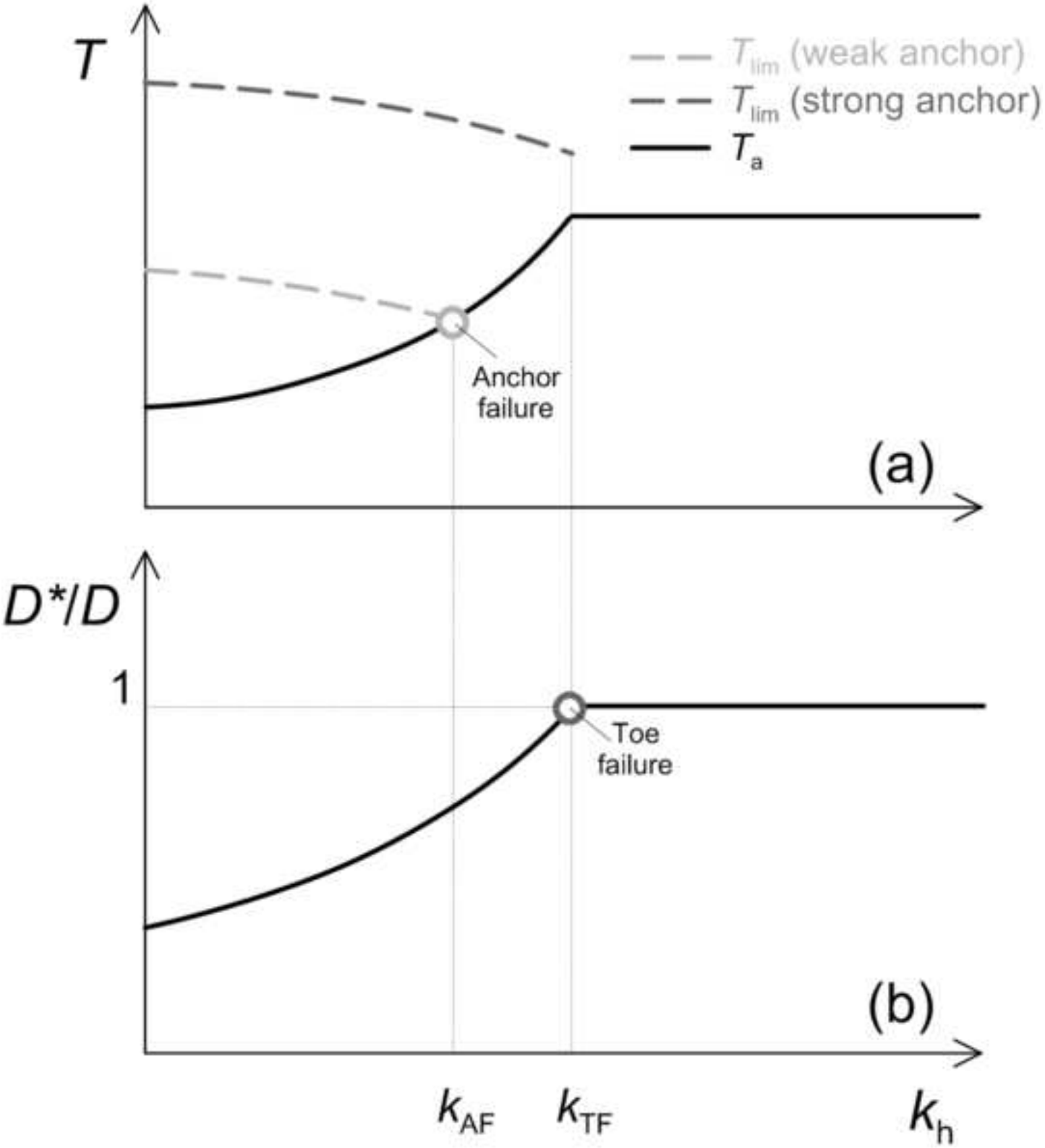

Figure 09

Click here to access/download;Figure;figure_09.tif

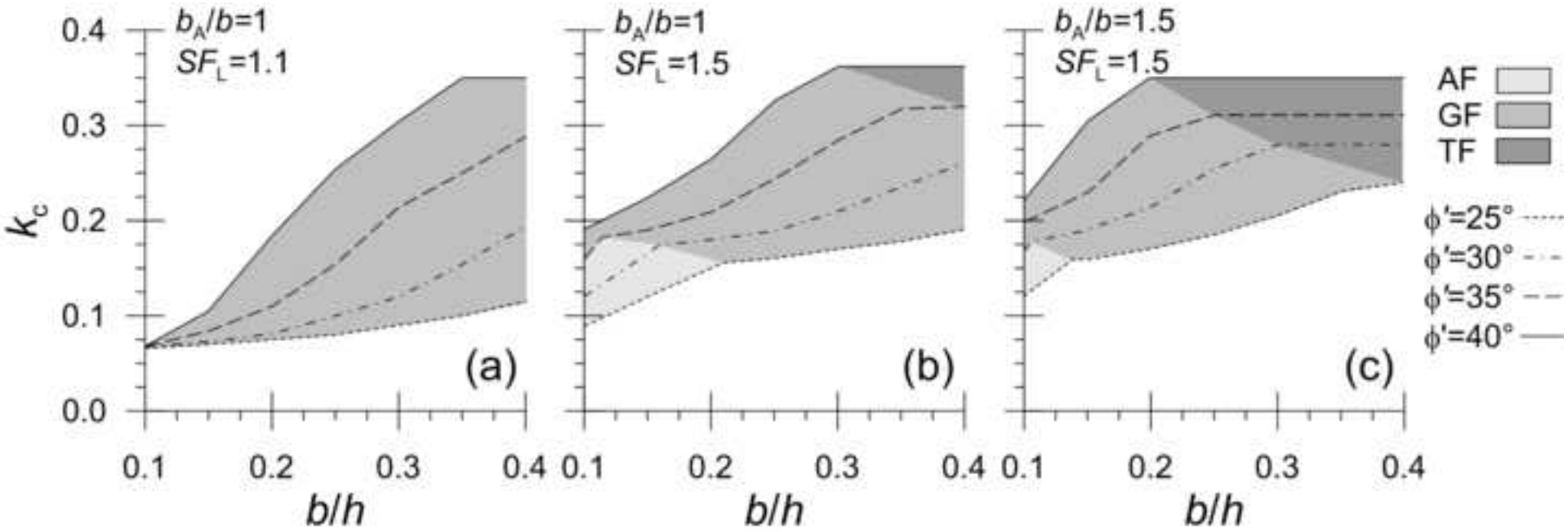

Figure 10

Click here to access/download;Figure;figure_10.tiff

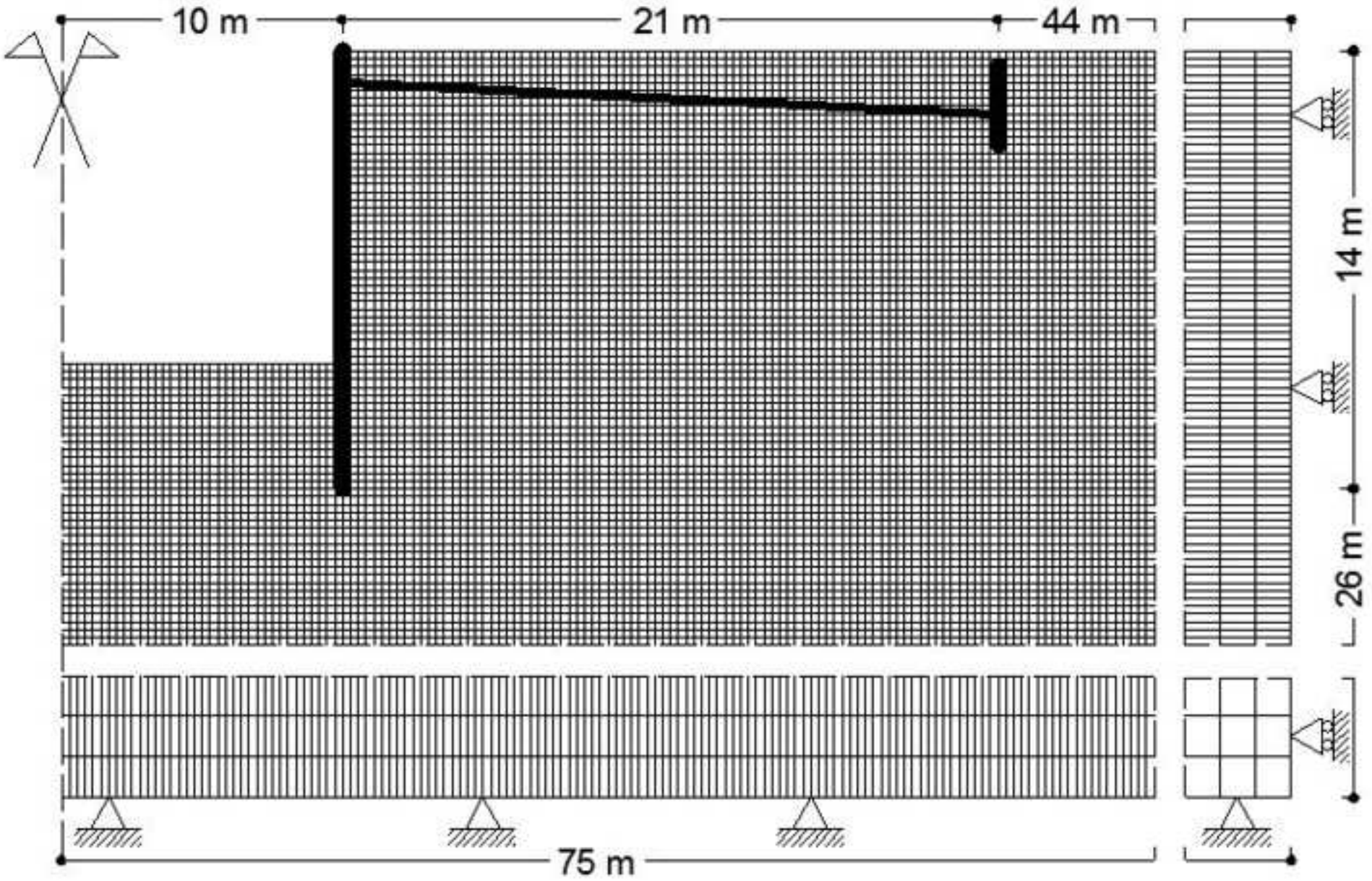

Figure 11

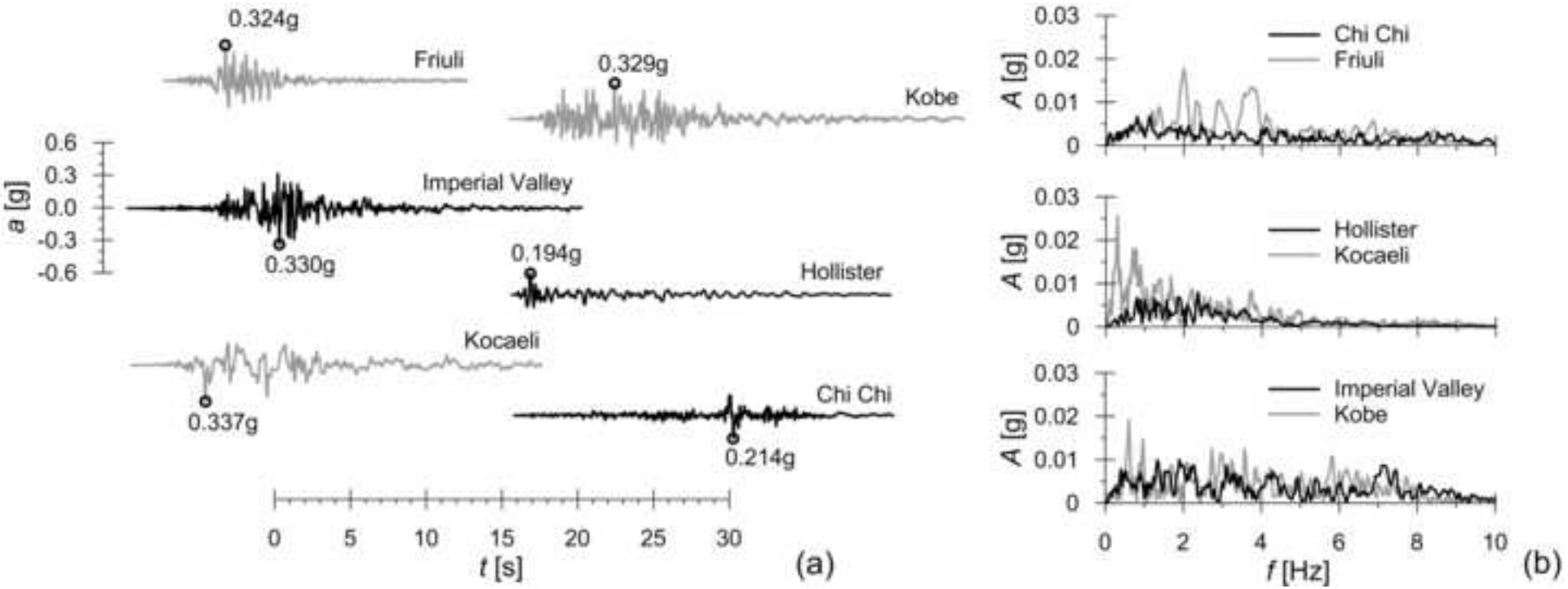

Figure 12

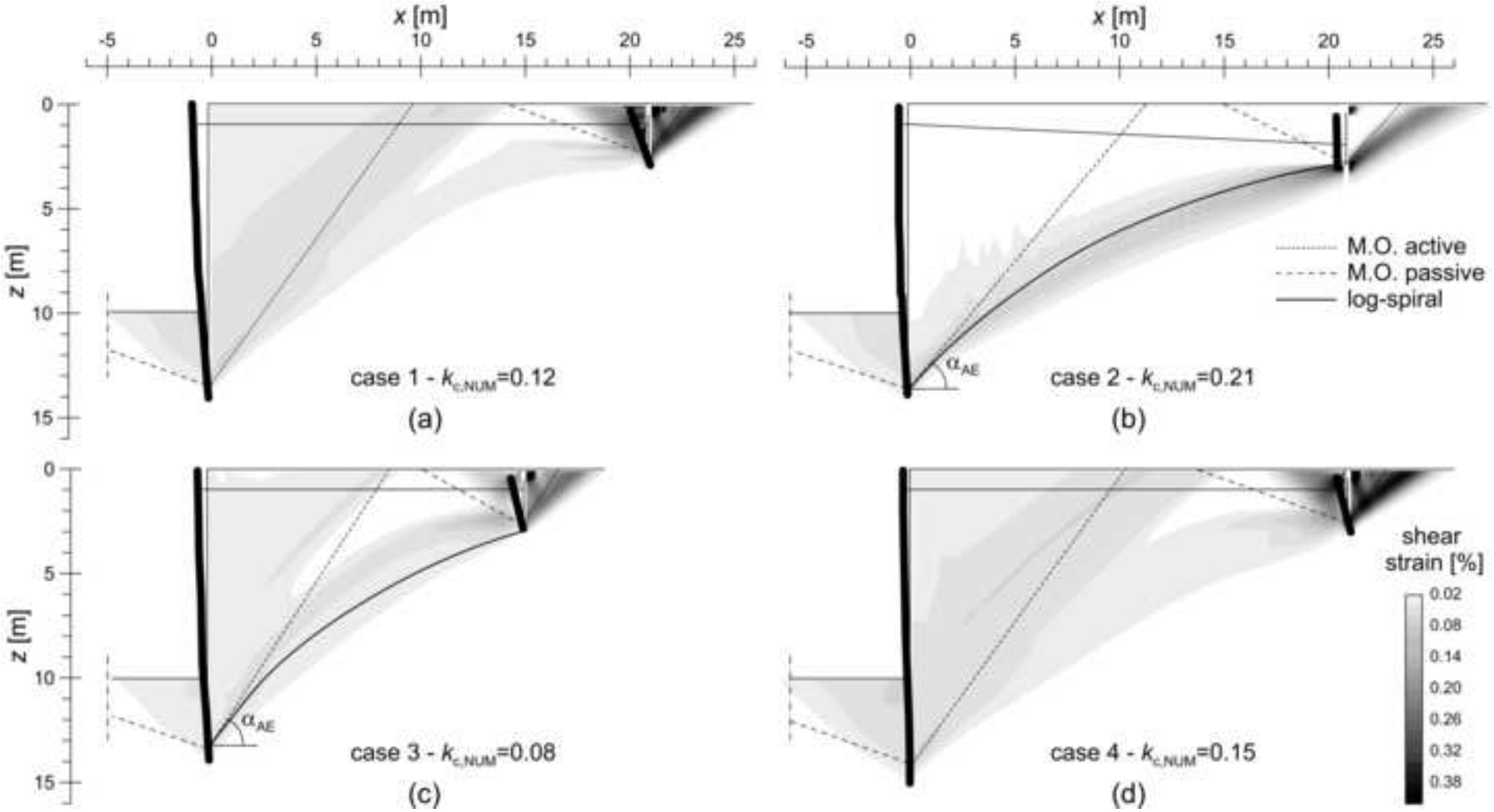

Figure 13

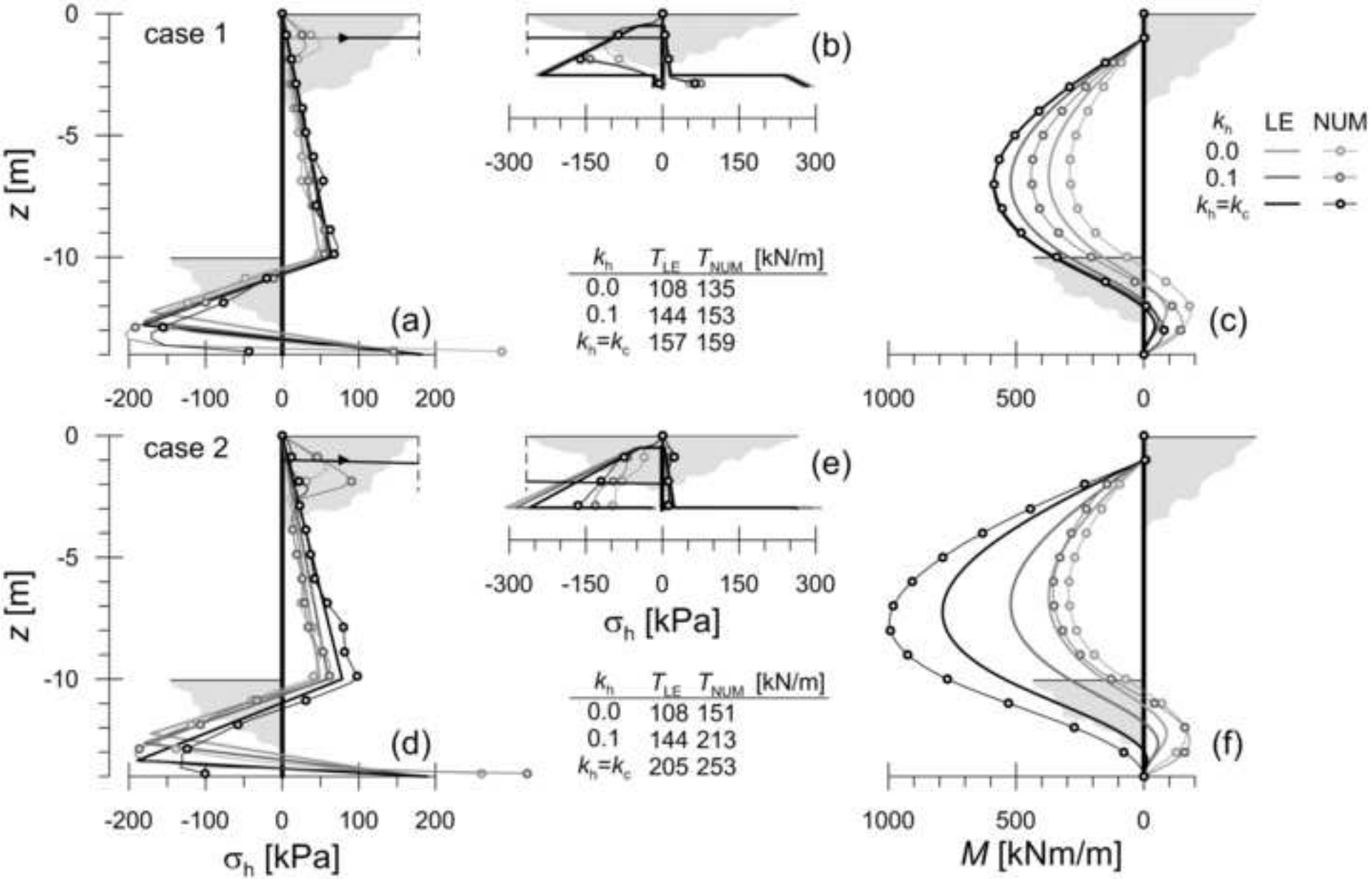

Figure 14

Click here to access/download;Figure;figure_14.tif

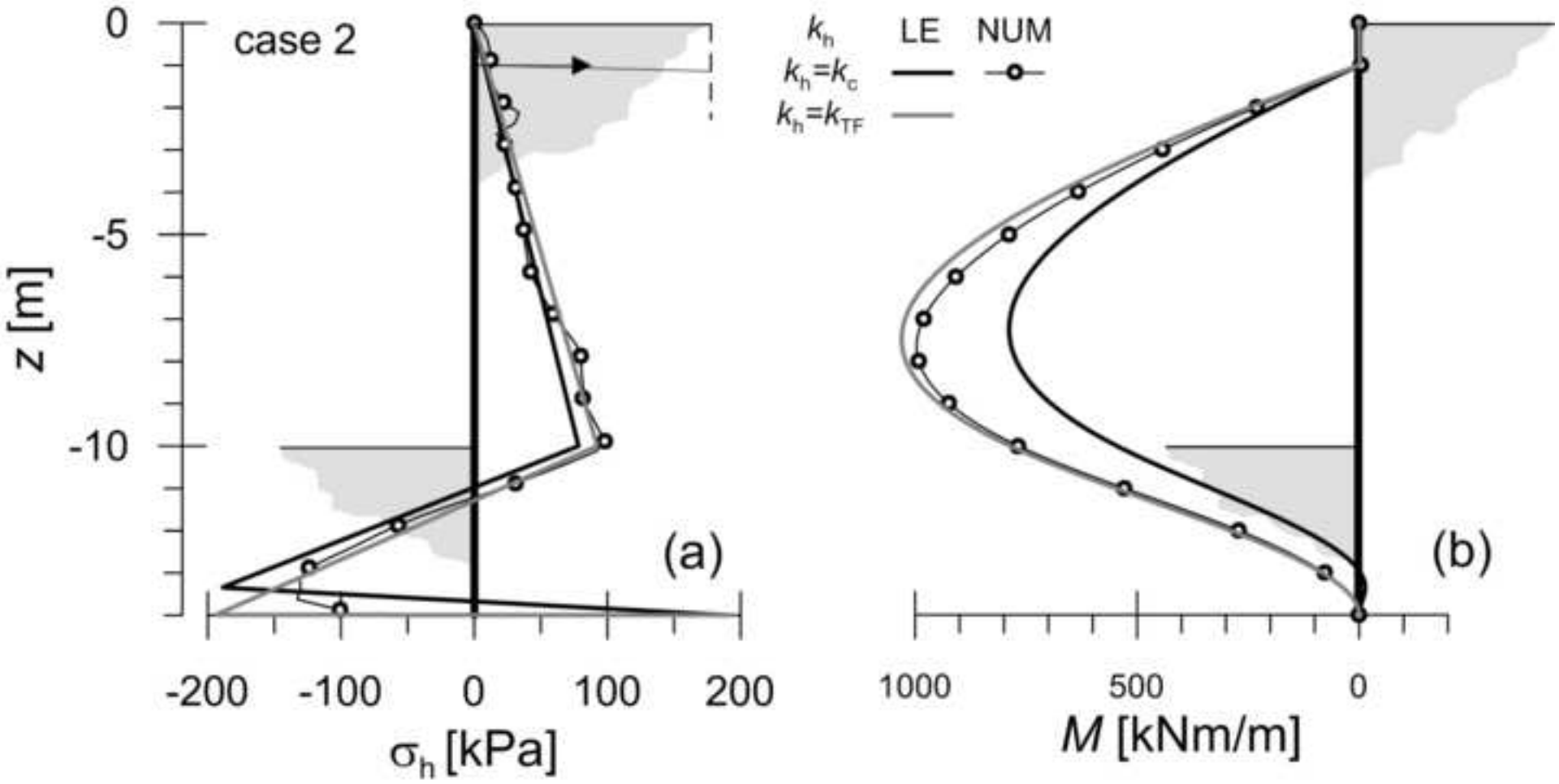

Figure 15

Click here to access/download;Figure;figure_15.tif

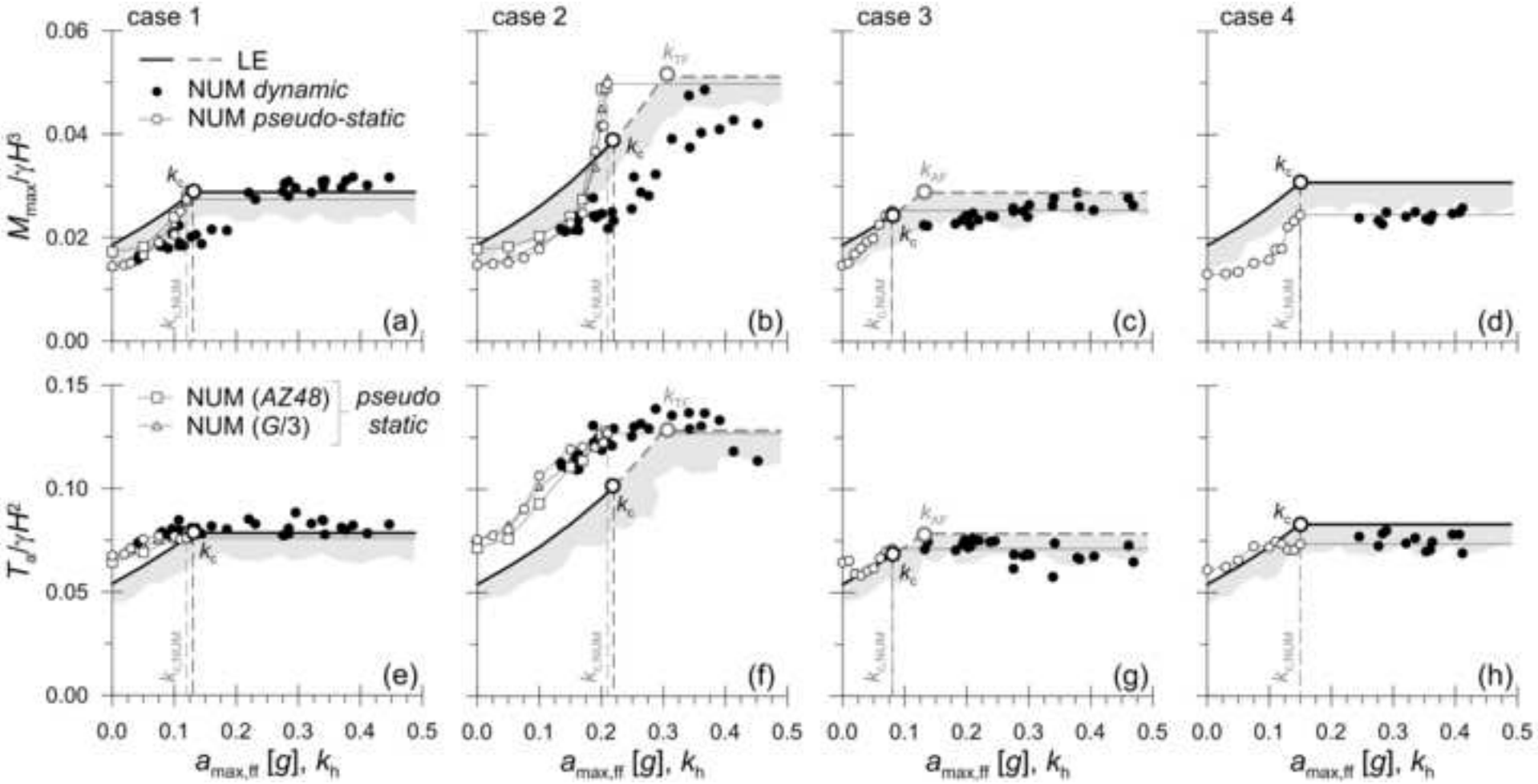

Figure 16

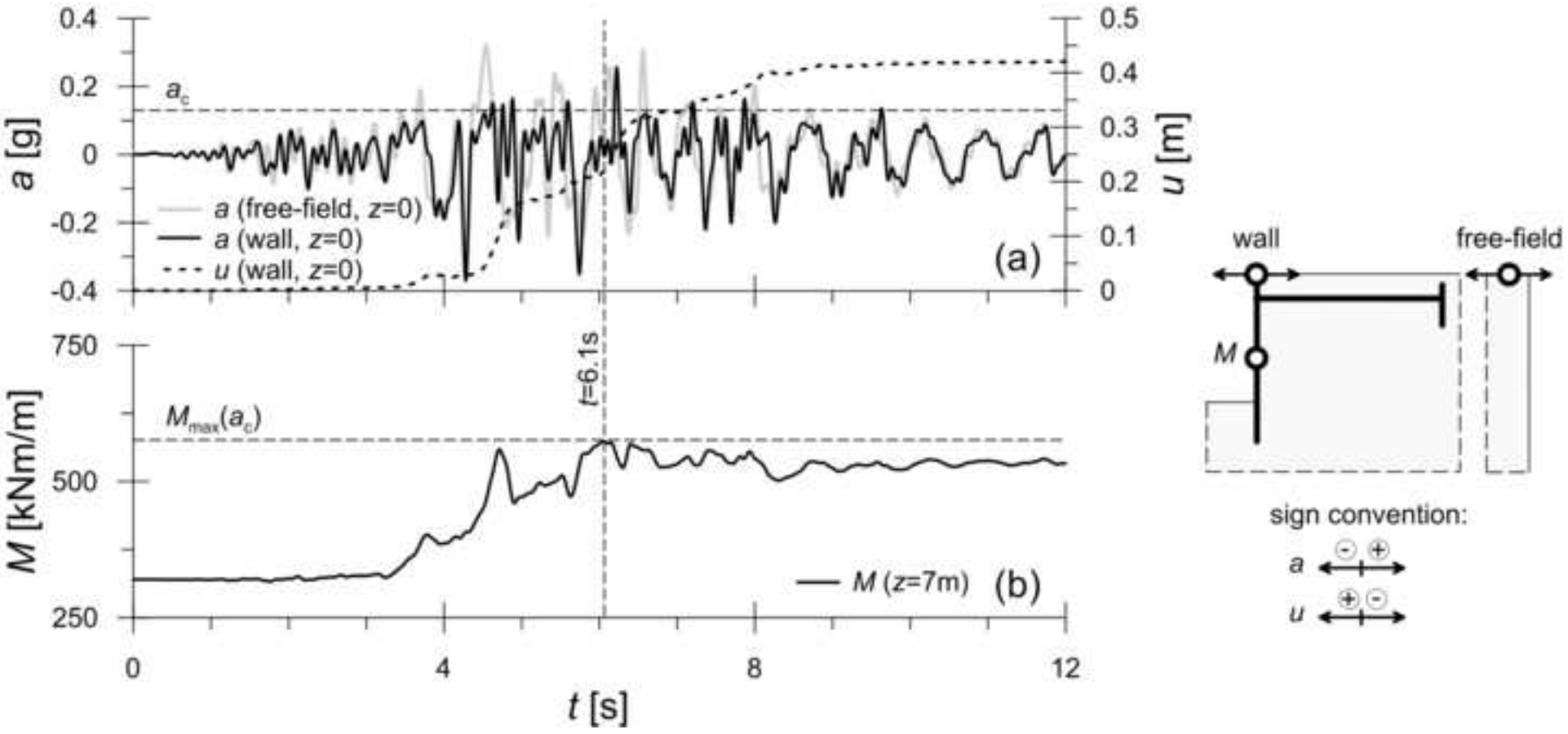

Figure 17

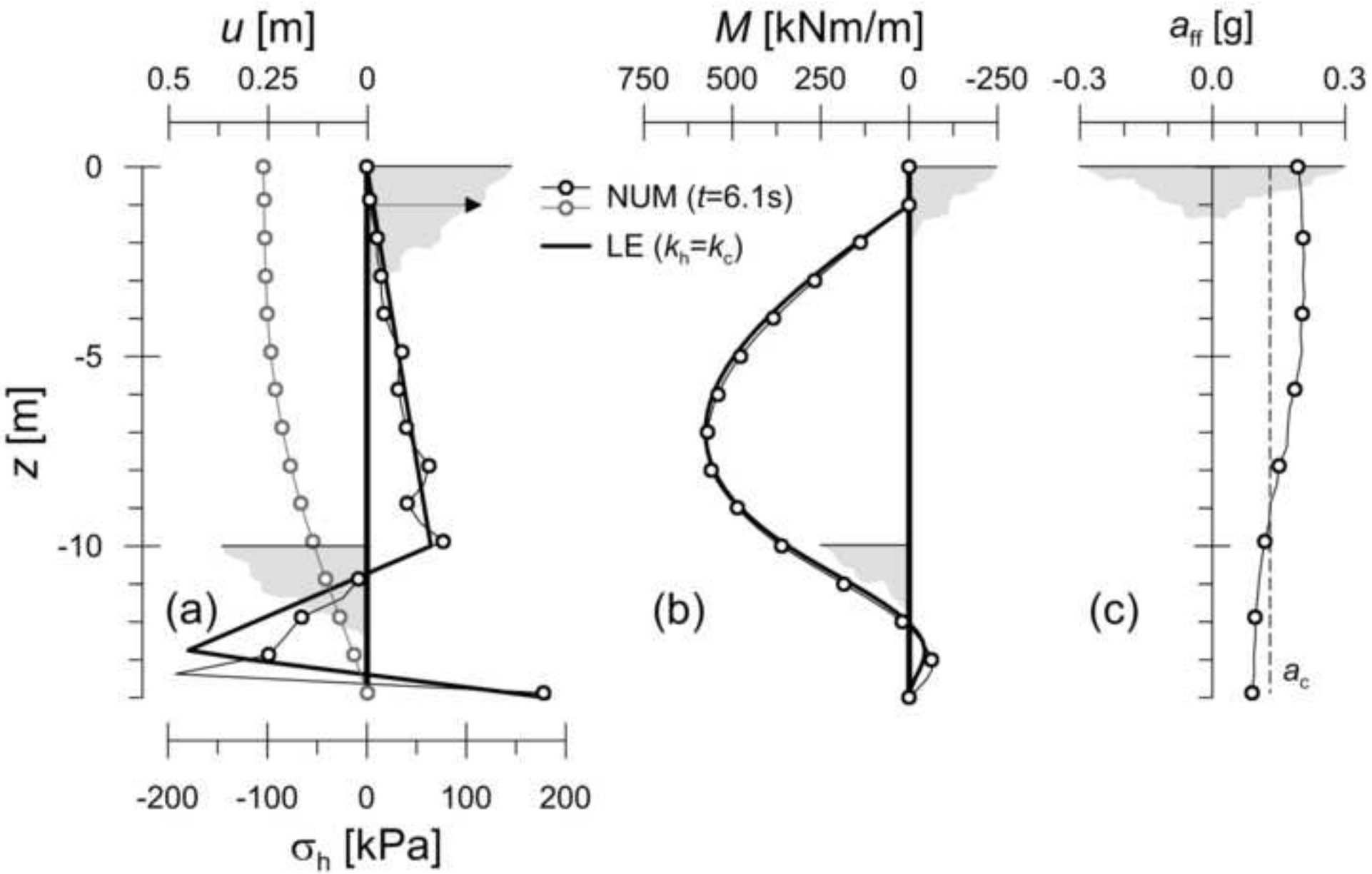

LIST OF FIGURES

LIST OF TABLES

Dr. Riccardo Conti
Associate Professor
Niccolò Cusano University
email: riccardo.conti@unicusano.it

Roma, May 7, 2020

Dear Editor,

attached please find a revised version of the paper (Ms. No. GTENG-8666):

"Principles for the balanced seismic design of anchored steel sheet pile walls"

by V. Giorgio Caputo, Riccardo Conti, Giulia M.B. Viggiani and Cécile Prüm

We read carefully the comments by the two Reviewers and the Associate Editor on the original submission and revised the work to take into account their remarks. This has led to a revised and improved version of the manuscript, including a change in the title, as suggested by the first Reviewer.

Following the Reviewers' comments, we have decided to integrate our original work with the results of full dynamic numerical analyses, where the four layouts of ASSP walls taken as reference in the original work were subjected to a number of real earthquakes, covering a wide range of amplitudes and frequency contents.

The comparison between the proposed pseudo-static approach and the numerical dynamic results provides further insight into the overall dynamic behaviour of ASSP walls and on their structural design, by strengthening some of the conclusions of our original work.

All the comments made by the two Reviewers are addressed in detail in the attached file.

Best regards,

Riccardo Conti

Detailed response to individual comments by reviewers:

The Authors wish to thank the Reviewers for their time, observations, and suggestions to improve the quality of the paper. A detailed response to their comments is given in the following. Any modifications in the revised paper are in blue text.

Reviewer 1

The paper treats a very challenging problem from the field of geotechnical earthquake engineering referring to the seismic response of flexible, embedded anchored retaining walls. The inherent complexity of the problem is due to the nonlinearity of soil behaviour, the interplay of earth pressure actions and resistances along the wall, and the strong dependency of earth pressures mobilisation on the pattern and amount of wall deformation. For these reasons, even for the static case, when using simplified analytical methods or beam on springs methods, various adjustments on the earth pressure distributions are made to account for the above mentioned effects. An alternative is the application of advanced constitutive models for the soils in connection with fully numerical methods. Even in that case particular attention is necessary in order to select a suitable soil model. For the seismic case the situation is even more complex.

Reviewer comment: 1. The title is not appropriate: For the reader is the meaning of a "balanced seismic design" not clear. There are "balance forces" when two forces acting in opposite directions on an object are equal in size. But what is a balanced design? Further, the paper describes a method not only the principles.

Acknowledged. The expression "balanced seismic design" refers to a design approach in which a balance is sought between all the possible yielding mechanisms and failure modes for a given structural system, typically adopted to achieve the desired strength hierarchy and prevent premature failure (see *e.g.* Roeder *et al*., 2005). This terminology was adopted by Neelakantan *et al*. (1992) to propose suggestions for the seismic design of anchored retaining walls. However, we agree with the Reviewer that it is not widely adopted and that it may be confusing and possibly even misleading, so we have decided to change the title of the manuscript, which now reads "An improved method for the seismic design of anchored steel sheet pile walls". For the same reason, we have removed any use of the expression "balance design" from the manuscript.

Reviewer comment: 2. The state of the art is more or less complete, although the relevant design methodologies are described in design codes. The authors mention papers adopting the Newmark's block analysis: but this is appropriate only for rigid gravity walls with a predefined rigid body failure mechanism. Even for this simple case of gravity walls that are loaded by active earth pressures the point of application of the resultant force is subject of research.

This is a very relevant point. As suggested also by Reviewer #3, Newmark's block analysis was originally introduced for rigid sliding slopes (Newmark, 1965) and then extended to sliding (Richards and Elms, 1979) and rotating (Zeng and Steedman, 2000) gravity walls. In recent years, more rigorous theoretical solutions have been proposed for the application of Newmark's procedure to sliding gravity walls (Conti *et al*., 2013; Biondi *et al*., 2014), while numerical, theoretical and experimental

works have dealt with the application of this procedure also in the case of other failure modes for gravity/cantilever walls (Conti *et al*., 2015; Kloukinas *et al*., 2015; Conti & Caputo, 2019).

Starting from the seminal work by Towhata and Islam (1987), a number of studies have proposed simple modifications to the classical Newmark method to assess the permanent seismic displacements also for of flexible embedded retaining structures, either cantilevered or with a single prop/anchor close to the top (Callisto and Soccodato, 2010; Conti *et al*., 2013, 2014; Callisto, 2019; Cattoni *et al*., 2019). Cattoni *et al*. (2019) have shown that a Generalised Newmark Method can be defined also for flexible yielding retaining structures, allowing the reconstruction of the full permanent displacement field around the excavation, and not just the evaluation of horizontal soil movements at selected points. A quite different approach has been recently proposed by Callisto (2019) for computing the seismic permanent displacement of both gravity and embedded retaining structures. The method is based on the application of a simple Single Degree Of Freedom model in conjunction with the critical acceleration concept, thus allowing to take into account, in a simple manner, both the stiffness (amplification) and strength (yielding) properties of the soil-structure interacting system.

The application of Newmark's analysis to the seismic design of flexible embedded retaining structures is also encouraged in seismic design guidelines (PIANC, 2001). However, we agree with the Reviewer that application of the Newmark's procedure to flexible embedded walls, among which ASSP walls, is still an open issue, given the multiple factors affecting their seismic behaviour. This point was explicitly addressed in the introduction of the manuscript.

We would prefer to maintain the reference to Newmark's approach in the Introduction of the paper, where both potentialities and issues of the method are explicitly addressed. However, following the Reviewer's comment, reference to the possible application of our results within a Newmark's type analysis has been removed in the revised manuscript, both in the Abstract and Conclusions (see also reply to Comment #5 of Reviewer #3).

Reviewer comment: 3. Line 65: define "strength of the system".

The expression "strength of the system" refers broadly to a measure of how far the system is from the failure condition, taking into account all the possible plastic mechanisms involving the structural elements and the soil interacting with them. In this sense, the strength of the system clearly depends on a number of factors, including: (i) the shear strength of the soil and the strength of the structural elements; (ii) the embedment depth of the main wall; (iii) the length of the tie rods; (iv) the eccentricity of the tie rods with respect to the anchor plate; (v) the height of the anchor plate. The role played by material strength, or point (i), is evident. Besides this, and broadly speaking: point (ii) determines the amount of passive strength mobilised in front of the main wall, thus affecting the plastic mechanism of toe failure; point (iii) is the major factor affecting the possible occurrence of a global plastic mechanism within the wall-soil-anchor system; points (iv) and (v) concur to determine the strength of the anchor system, thus playing the major role in the plastic mechanism of anchor failure.

All these points are thoroughly discussed in the manuscript. At this stage, as we are just introducing the most relevant points from the literature, we would prefer to maintain the text as general as it is in the present form. However, following the Reviewer's comment, we have slightly changed the manuscript, which now reads: "*[…] overall strength of the system […]*".

Reviewer comment: 4. Line 93: proper construction and design shall avoid liquefaction.

Acknowledged. We agree with the Reviewer that proper design should avoid liquefaction. However, in order to achieve this result, the possible occurrence of pore pressure build-up, eventually leading to liquefaction of the backfill and of the supporting soil, must be properly assessed at the design stage. Furthermore, occurrence of partial liquefaction has been documented in port structures also during recent earthquakes (see *e.g.*, Sumer *et al*., 2007; Sugano *et al*., 2014). Following the Reviewer's comment, we have removed the reference to liquefaction from the text, which now reads: "*[...] possibly leading to pore pressure build-up within the soil [...]*". Anyhow, as explicitly stated at the end of the Introduction, our work deals only with dry sand, neglecting any effects of pore pressure build-up during shaking.

Reviewer comment: 5. Starting in line 96 the authors define their ambitious task: "... a new pseudo-static LE method is presented for the computation of: (i) the maximum internal forces in the structural members; (ii) the anchor capacity; and (iii) the pseudo-static accelerations inducing local or global plastic mechanisms within the soil interacting with the retaining structure". Indeed, these are the challenges.

Indeed.

Reviewer comment: 6. Line 99: replace "balanced approach" with something more appropriate.

Acknowledged. We have changed "balanced approach" with "strength-hierarchy approach" in the revised manuscript (see also the reply to Comment #1).

Reviewer comment: 7. In line 116 three possible failure mechanisms are introduced. For each of them a critical value of the seismic coefficient is determined. In §2.1 the distribution of the earth pressures, both active and passive is defined. However, the depth-profile depends on the assumed deformation pattern. This is the crucial assumption, even for the static design. For an economical design the assumptions for static and seismic design should be compatible.

The assumptions introduced for the active and passive earth pressure distributions in static and seismic conditions are fully compatible. As an example, Figure 13 of the revised manuscript compares the contact pressures on the main wall and on the anchor plate, obtained using the proposed approach for $k_h = 0$ (static condition) and k_h increasing up to its critical value.

Regarding the dependence of the contact pressure-depth profile on the deformation pattern, see reply to Comment #8.

Reviewer comment: 8. Line 135: There is a huge difference in deformation patterns between cantilever and anchored walls.

We agree with the Reviewer that the deformation patterns of embedded cantilevered and anchored walls are not exactly the same. As a matter of fact, as discussed in the manuscript (see *e.g.*, § 2.1 and 4.2), the overall kinematics in the two systems is different due to the presence of the constraint provided by the tie rod in the case of anchored walls.

However, considering that in the case of passive anchorages a certain amount of displacement is always needed to activate the required resistance, the progressive mobilization of soil passive strength below dredge level is always initially associated with a rotation of the main wall around a pivot point

close to the toe, just as in the case of cantilever walls. This evidence was observed both experimentally and numerically (see *e.g.* Zeng and Steedman, 1993; Gazetas *et al*., 2016, Fusco *et al*., 2019).

In addition to this, taking into account also the flexibility of the main wall, the earth pressure distribution at the contact between the soil and the wall is very similar between cantilever and anchored walls, with the only exception of the soil located close to the anchor connection. Apart from this zone, in both cases the contact pressure distribution suggests that the soil has reached active limit state in most of the supported soil, and passive limit state in the supporting soil, at least immediately below dredge level. On both sides, the depth down to which the soil strength is fully mobilised depends on the embedment depth (static condition) and on the applied horizontal acceleration (seismic condition). This is the reason why the theoretical pseudo-static contact stress distribution proposed in this work was "inspired" by other works carried out on cantilever walls, as explicitly stated in the manuscript.

The similarity in the contact stress distributions between cantilever and anchored walls was confirmed, both in static and dynamic conditions, by a number of numerical works on embedded retaining walls. In addition to the present work, reference can be made to Callisto *et al*. (2008), Conti (2010), Cilingir *et al*. (2011) and Bilgin (2012) for anchored and propped walls, and to Madabhushi and Zeng (2007), Callisto and Soccodato (2010), Conti (2010), Conti *et al.* (2014) and Conte *et al*. (2017) for embedded cantilever walls.

Just as an example, Figure A shows a qualitative comparison between the horizontal contact stress distributions computed numerically for a pair of (a) embedded cantilever walls and (b) single-propped walls (after Conti, 2010). The numerical results refer to the simulation of two centrifuge dynamic tests carried out on a pair of cantilever and propped walls embedded in dry sand (Conti *et al*., 2012). The analyses were carried out with the FDM code FLAC, using an advanced constitutive model for the soil (Andrianopoulos *et al.*, 2010a, b). The comparison shows a very similar trend in the stress distributions, with a progressive mobilization of the soil passive strength in front of the wall, with increasing shaking level, and a concurrent increase of the soil active pressure behind the wall. As anticipated, the presence of the prop imposes a very stiff constraint to the lateral movements of the two facing walls, thus inducing a local increase of the soil pressure behind the prop connection. In the case of anchored walls, where the passive anchorage allows for a some amount of wall displacement, a less pronounced increase of the soil pressure behind the wall should be expected, as observed in the present work (see *e.g*., Figure 13 of the revised manuscript).

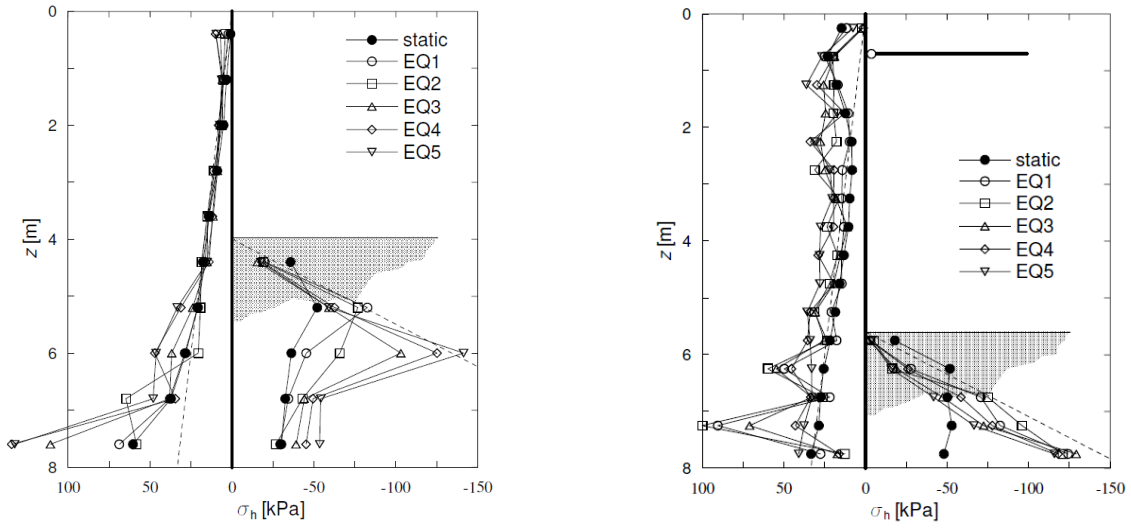

Figure A. Horizontal contact stress distributions computed numerically in static conditions and under different input earthquakes: (a) pair of embedded cantilever wall; (b) pair of single propped retaining walls (modified after Conti, 2010).

Reviewer comment: 9. Line 140: "the soil passive strength is fully mobilised in the supporting soil": this is not realistic since this would require a large movement. How is the ratio D/depth Do determined? Earth pressure coefficients were determined according to Mononobe-Okabe?

The text reads: "*[…] On the retained side, the soil is in active limit state down to D^*; along the same depth, the soil passive strength is fully mobilised in the supporting soil […]*". In other words, as shown also in Figure 1 of the manuscript, the proposed method assumes that the passive strength in front of the wall is fully mobilised down to a depth D^* below dredge level. As stated in the paper, the depth D^* and the anchor force T_a are the two unknowns in the proposed force diagram, and they can be computed by solving the two equilibrium equations of the wall.

The assumption on the earth pressure distribution in front of the wall is consistent with the results of a number of numerical works dealing with the static and dynamic behaviour of propped and anchored retaining walls (*e.g.*, Bilgin, 2010, 2012; Callisto *et al*., 2008; Conti, 2010; Gazetas *et al*., 2016). As a matter of fact, the full mobilization of the soil passive pressure down to D^* is a result of three concurrent phenomena; (i) the wall flexibility; (ii) a small amount of outwards rigid wall movement; (iii) soil dredging in front of the wall (when carried out), naturally leading the remaining soil to a passive limit state by the induced overconsolidation.

Regarding the earth pressure coefficients, Mononobe-Okabe solution was used to compute the active earth pressure coefficient (K_{AE}), while the lower-bound solution proposed by Lancellotta (2007), which is inherently conservative, was used to compute the passive pseudo-static earth pressure coefficient (K_{PE}). Following the Reviewer's comment, we have slightly rewritten this part of the original manuscript in order to make this point clearer.

Reviewer comment: 10. In §2.2: method M1 requires the definition of SF, which in turn requires knowledge of the passive earth pressure mobilisation function. Method M2 assumes rigid rotation of the wall that is not realistic.

Both method M1 and method M2, are published in the literature (Neelakantan *et al*., 1992; Zeng and Steedman, 1993). The two methods are used as reference to highlight the predictive capabilities of the proposed pseudo-static LE method.

Method M1 (Neelakantan *et al*., 1992) assumes that a constant fraction $1/SF_P$ of the soil passive strength is mobilised in front of the wall. The resulting force diagram, shown in Figure 2(a), is completely defined by the two unknowns T_a and SF_P, which can be determined by solving the two equilibrium equations of the wall.

Method M2 was originally proposed by Zeng and Steedman (1993), based on the observation that damages to port structures during real earthquakes are frequently associated to tilting of the sheet piles towards the sea. This observation, which was further confirmed by a number of centrifuge tests carried out by the same Authors on reduced scale models of anchored walls in dry and saturated sand, is clearly related to the fact that passive anchorages do not provide a perfect (fixed) constraint to the wall movements at the connection with the tie rod (see also reply to Comment #8 raised by the Reviewer).

<u>Reviewer comment:</u> *11. Figure 3a compares the three methods/options. Are the three ratios used comparable? Is Dstar/D equal to 1/SF? It would be helpful for the reader to provide numerical values. Are the curves valid for all ratios H/D? The wall design aims at optimizing the embedment depth. Are the results for the proposed method ignoring the anchor plate? Model M1 assumes a sudden drop of the pressures on the wall at the level of the wall toe. The drawbacks of method M2 are described in the text.*

As stated in the text, Figure 3 was plotted for a specific set of parameters and layout of the wall, *i.e.*, $\gamma = 20$ kN/m^3, $\phi' = 35°$, $\delta = \phi'/3$, $D/H = 0.5$, $b/H = 0.1$. The value of $D/H = 0.5$ was chosen as the midpoint of the range of credible values for ASSP walls, $D/H = 0.4$-0.6. For the sake of clarity, in the revised manuscript we have added the indication of the layout parameters also to the caption of Figure 3. Moreover, the figure now displays also the values of k_{TF}, $M_{max}(k_{TF})$ and $T_a(k_{TF})$, *i.e.*, the value of the pseudo-static acceleration corresponding to toe failure, and the corresponding values of maximum bending moment and axial force, which are the same for all three methods.

Figure 3 shows (synthetically) the evolution of the contact stress distribution with increasing k_h and the resulting internal forces, as predicted by the three methods. The three ratios reported in Figure 3(a) - *i.e.* D^*/D (proposed method), $1/SF_p$ (Method M1) and D_0/D (Method M2) - are clearly not the same numerically, but they have the same conceptual meaning. In fact, they are all measures of the distance of the system from collapse by full mobilisation of the passive strength in front of the wall, each consistent with the corresponding method of analysis. Please note that the continuous line in Figure 3(a) has been changed in the revised manuscript, as we realised that this curve, referring to the proposed method, was representing the ratio D_0/D instead of D^*/D, as declared in the text.

As the degree of mobilization of soil passive strength in front of the wall depends physically on the embedment depth of the wall, the curves displayed in Figure 3 would be different in the case of different D/H ratios, but the trend with increasing k_h would be exactly the same. This is clear by inspection of Figure B, showing the same curves displayed in Figure 3(a) for three values of $D/H = 0.4$, 0.5 and 0.6.

Finally, the proposed method takes into account both the main wall and the anchor plate, but in two different stages. Sections 2.2 refer to the pseudo-static design of the main wall, while Section 2.3 addresses the problem of the seismic design of the anchor system.

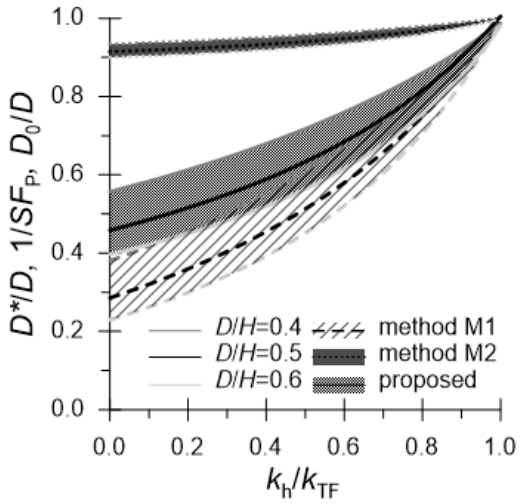

Figure B. Comparison between pseudo-static LE methods in terms of mobilised passive strength in front of the wall, for different D/H ratios (γ = 20 kN/m^3, ϕ' = 35°, $\delta = \phi'/3$, b/H = 0.1).

<u>Reviewer comment:</u> 12. Figure 4 displays the bending moments. The bending moment in the wall at the level of the anchor is zero, that cannot be correct. Method M1 and M2 provide contradictory results: bending moments of opposite signs. Do the results from method M2 show such a large deviation from their own experiments? For the reader, this figure is so confusing that he immediately rejects all methods proposed. At the latest in this point he will stop reading the paper. The authors should comment on this, and if one of the methods is inacceptable it should be removed. Are the scaling laws to transfer the results from the centrifuge tests fulfilled?

Experimental and theoretical bending moments shown in Figure 4 refer to the centrifuge tests discussed by Zeng and Steedman (1993) (all the data reported by the Authors were given directly at prototype scale or in non-dimensional form). As observed by the Reviewer, the bending moment at the level of the anchor is not zero, but small compared to the maximum value computed along the wall and hence barely visible in Figure 4 of the manuscript. This is evident by inspection of Figure C, showing a detail of the bending moment computed close to the anchor.

In their paper, Zeng and Steedman (1993) compared their centrifuge results and the predictions of their method (M2) without stating the adopted value of the friction angle at the contact between the soil and the wall, δ. The curves published in their paper can only be obtained if a value $\delta = 0°$ is used. A realistic value of $\delta = 12°$ was measured by Madabhushi and Zeng (2007) for the contact friction angle between the Leighton Buzzard sand and the aluminium sheets used to model the retaining walls. Indeed, the results reported in Figure 4 of our original manuscript were obtained using $\delta = 12°$ in all LE calculations, as explicitly stated in the paper. This was motivated by the fact that any Limit Equilibrium method would be used in the design practice together with a realistic assumption on the soil-wall contact friction angle. However, we understand (and share) the Reviewer's concern that we were somehow misrepresenting the original work by Zeng and Steedman (1993), and decided to modify Figures 4 and 5 of the original manuscript, and related comments, by adding also the theoretical results published by Zeng and Steedman (1993) using $\delta = 0°$.

We agree with the Reviewer that methods M1 and M2 provide contradictory results, as they predict maximum bending moments of opposite sign (but similar in magnitude). This result is related to the different assumption on the contact earth pressure distribution. Moreover, both methods lead to a gross overestimation of the magnitude of the maximum bending moment measured in the centrifuge experiments.

The comparison of the proposed method with methods M1 and M2 from the literature allows to highlight the better performance of the proposed method with respect to other published approaches. This result should be clear from Figures 4 and 5 of the manuscript, where the proposed method shows a very good agreement with the centrifuge results. Indeed, only the proposed method is used and discussed in the following sections of the manuscript, thus implicitly embracing the suggestion by the Reviewer that "[…] if one of the methods is inacceptable, it should be removed […]".

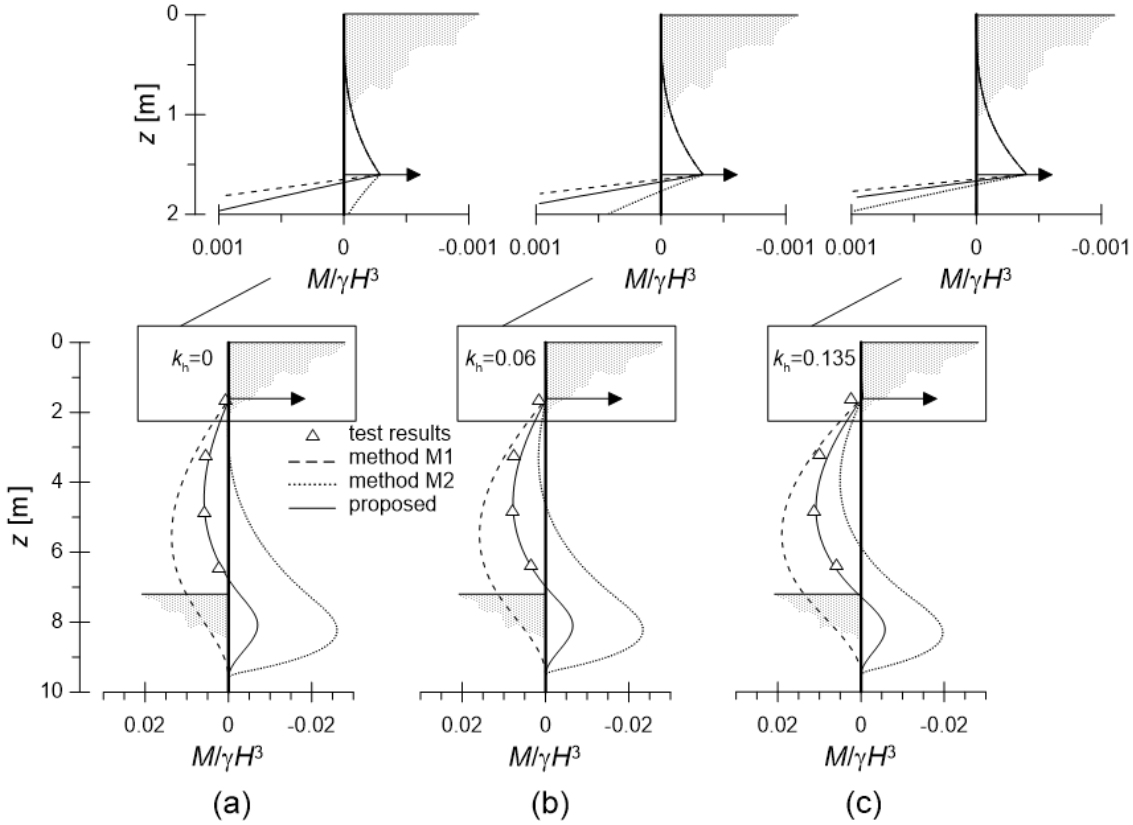

Figure C. Dynamic centrifuge test results published by Zeng & Steedman (1993). Comparison between experimental data and theoretical LE predictions of bending moments for: (a) k_h = 0 (static); (b) k_h = 0.06 g; (c) k_h = 0.135 g.

<u>Reviewer comment:</u> *13. §2.3 addresses the anchor capacity. Do the earth pressure coefficients include seismic action? T_lim is the limit load. The term "balanced anchor condition" needs clarification. T_lim: The plate is loaded by the anchor force from the seismically excited wall, by the enhanced active pressure on the right hand side of the plate and the reduced earth pressure beneath the rotation point whereas support is provided by the mobilised passive earth pressure. The mobilisation of the full passive earth pressure requires a movement that is provided either by the elongation of the anchor that then must decay to zero at the wall. Is this assumption realistic?*

The theoretical earth pressure distribution assumed to compute the seismic capacity of the anchor is given in Figure 1(b) of the paper, where K_{AE} and K_{PE} are the pseudo-static earth pressure coefficients corresponding to an active and passive limit state, respectively (see also reply to Comment #9 raised

by the Reviewer). Therefore, the earth pressure coefficients do include the seismic action, through the standard horizontal pseudo-static coefficient, k_h.

As thoroughly discussed in reply to Comments #8, #9 and #10 raised by the Reviewer, in the case of passive anchorages a certain amount of displacement is always needed to activate the required anchor force, which reflects in outwards movements of both the main wall and the anchor plate. This evidence was confirmed by both numerical analyses and field observations of the seismic performance of ASSP walls during real earthquakes. Clearly, any difference in the horizontal displacement between the main wall and the anchor plate, computed at the tie-rod level, must be ascribed to the elongation of the tie-rods, which is typically small compared to the overall wall movements (just as an example of design solution, a working load of 1250 kN in a tie rod with a diameter of 90 mm and a length of 33 m, would produce an elongation of 3.1 cm (AM Manual, 2009)).

Anyway, it is worth mentioning that T_{lim} is the anchor capacity, not the axial load effectively acting in the tie rods (T_a). The condition $T_a = T_{lim}$ applies only when the plastic mechanism activated by the earthquake corresponds to a full mobilization of the anchor capacity (anchor failure). In other words, for horizontal accelerations lower than the pseudo-static value corresponding to the activation of this mechanism ($k_h < k_{AF}$), the axial force in the tie rods is lower than T_{lim} ($T_a < T_{lim}$), so the actual amount of soil pressure mobilised in front of the anchor plate is lower than the passive strength required to balance T_{lim}. This is confirmed also by the numerical results discussed in Figure 13 of the revised manuscript where, for $k_h < k_{AF}$ (see *e.g.* Figure 13b, e), the horizontal stresses computed in front of the anchor plate are well below the passive limit values corresponding to $T_{lim}(k_h)$.

Regarding the expression "balanced anchor condition", we have removed this expression from the revised manuscript, which now reads more simply: "*[…] with the upper bound provided by the condition $b_A/H_A=2/3$, corresponding to which a pure triangular contact stress distribution is obtained […]*". The kinematics of the anchor plate depends on the ratio b_A/H_A, representing the eccentricity of the anchor force with respect to the anchor plate. The condition $b_A/H_A = 2/3$ corresponds to a pure triangular distribution of the soil contact stresses, which is statically equivalent to the contact stress distribution for a pure translation of the anchor. We have tried to enhance this by showing schematically the contact stress distribution corresponding to different values of b_A/H_A in Figure 6.

<u>Reviewer comment:</u> *14. Line 232: What is weak anchor? Why does D*/D < 1 imply mobilisation of full passive earth resistance? What degree of mobilisation prevails?*

The expressions weak and strong anchor refer to the overall seismic capacity (strength) of the anchor system and their definition were given (implicitly) in the text. Following the Reviewer's comment, we have modified the original manuscript to make this point more clear. The text now reads:

"*[…] With increasing k_h, two limiting situations are possible:*

1) *in the case of a weak anchor, local attainment of the anchor capacity ($T_a = T_{lim}$ for $k_h = k_{AF}$) precedes complete mobilization of the soil passive strength; therefore, in this case we have $D^*/D < 1$;*
2) *for a strong anchor, complete mobilization of the soil passive strength below dredge level ($D^*/D = 1$ for $k_h = k_{TF}$) is achieved before anchor capacity is attained, for $T_a < T_{lim}$. […]*"

It should be clear, from the revised text, that full mobilization passive earth resistance in front of the main wall corresponds to the condition $D^*/D = 1$.

<u>Reviewer comment:</u> *15. Line 234 states that for a strong anchor, that is for the condition of Figure 1a, we have Dstar/D = 1. This means that the rotation point moves down with increasing seismic level. This in turn will require a deeper embedment.*

Figure 8 (and the related comment) refer to the two local plastic mechanisms of anchor failure and toe failure. The first mechanism occurs in the case of a weak anchor system, while the second one takes place in the case of a strong anchor system (see also reply to Comment #14). The theoretical distribution of soil pressures at the onset of the two local mechanisms is displayed in Figure 7a (toe failure) and in Figure 7b (anchor failure). Figure 1a, instead, refers more generally to the assumed earth pressure distribution for $k_h < k_c$, *i.e.*, before a local plastic mechanism is attained into the system.

As observed by the Reviewer, the rotation point in Figure 1a moves downwards with increasing pseudo-static acceleration. The condition $D^* = D_0 = D$ corresponds to the complete mobilization of the soil passive strength in front of the wall, which is referred to as toe failure in our work ($k_h = k_{TF}$). As performance-based approaches do allow for the accumulation of permanent displacements during the design earthquake, the attainment of the condition $D^* = D$ will not require necessarily a deeper embedment, as explained in the following.

The geotechnical seismic design of ASSP walls consists in verifying the seismic performance of the wall, essentially in terms of embedment depth and anchor system. PBD approaches, in the form of both Force-based (pseudo-static) and Displacement-based (simplified dynamic) methods, admit that the retaining structure can experience permanent displacements during an earthquake, provided that the associated damage does not exceed some allowable threshold, defined on the basis of a given required performance level. In other words, PBD approaches acknowledge that the strength of the system can be fully mobilised during the design earthquake and, therefore, that the critical acceleration of the wall ($a_c = g \cdot k_c$) can be lower than the peak ground acceleration expected at the reference site ($PGA = g \cdot k_{h,max}$). According to this, the design requirement to assess the seismic performance of the wall is:

a) When using a Force-based (pseudo-static) method: $k_{h,eq} < k_c$, where $k_{h,eq} = \beta \cdot k_{h,max}$ and $\beta \leq 1$ is a reduction coefficient which takes into account the possibility for the wall to experience permanent displacements during the design earthquake (see *e.g.* Anderson *et al.*, 2008; NTC, 2018). According to this method, the wall must be in equilibrium under the equivalent pseudo-static coefficient $k_{h,eq}$.
b) When using a Displacement-based (simplified dynamic) method: $u < u_{adm}$, where u is the permanent displacement induced by the design earthquake and u_{adm} is the allowable threshold (see *e.g.* Steedman, 1998; NTC, 2018).

In case (a), as the wall must be in equilibrium under the pseudo-static coefficient $k_{h,eq}$, the condition $D^* < D$ must be fulfilled for $k_h = k_{h,eq}$, as argued by the Reviewer (however, this will not be the case for $k_h = k_{h,max}$).

In case (b), the wall is assumed to be a displacing wall. Then, if $k_c = k_{TF}$, the wall moves only if $k_{h,max} > k_{TF}$, that is only if the condition $D^* = D$ is attained.

<u>Reviewer comment:</u> *16. Line 290: Check units of density or is it a unit weight?*

Acknowledged. It is a unit weight. We corrected the error in the revised manuscript.

<u>Reviewer comment:</u> *17. Line 383: Based on a theoretical parametric study, it was concluded that for typical layouts of ASSP walls the most likely failure mechanisms are local anchor failure and global failure: This should not be generalized: The crucial assumption is that the entire system is excited by a constant pseudo-static force. Due to this in-phase excitation and the large extent of the considered rigid soil body the inertial forces are huge. Furthermore, the seismic coefficient should include some reduction factor, it cannot be the same as for immovable walls.*

The outcomes of the theoretical (pseudo-static) parametric study were confirmed by fully-dynamic numerical FDM analyses, where typical layouts of ASSP walls were subject to a number of real earthquakes, covering a wide range of amplitudes and frequency contents (see also reply to Comment #6 raised by Reviewer #3). Anyway, following the Reviewer's comment, we have changed this point of the Conclusions in the revised manuscript, which now reads: "*[…] Based on a theoretical parametric study, carried out under pseudo-static conditions, it was concluded that for typical layouts of ASSP walls the most likely failure mechanisms are local anchor failure and global failure […]*".

With reference to this point, it is worth mentioning that the good agreement between pseudo-static limit equilibrium calculations and dynamic numerical analyses - in terms of contact earth pressure distributions, internal forces in the structural members and critical plastic mechanism - was obtained also from other numerical works on embedded cantilever walls (Callisto and Soccodato, 2010; Conti *et al*., 2014).

Regarding the choice of the pseudo-static coefficient to be used in pseudo-static calculations of displacing walls, $k_{h,eq}$, please see the reply to Comment #15 of the Reviewer.

<u>Reviewer comment:</u> *18. Line 385: Before making this statement, the authors should check again the geometry/stiffness of the wall corresponding to the centrifuge model and the bending moment distributions in Fig. 4.*

As shown in Figures 4 and 5 of the manuscript, the proposed method is in very good agreement with the centrifuge data (see also the reply to Comment #12 of the Reviewer).

<u>Reviewer comment:</u> *19. Summing up, the paper presents an interesting approach for the calculation of seismic response of plate anchored walls typically installed in waterfront structures. Still the method proposed needs refinement and clarification of some of the assumptions made, as outlined above. Methods that provide wall sectional forces that are not realistic should be removed. Figures 4 need correction. The issue of passive earth pressure mobilisation should be addressed in more detail in an amended version. The paper should be re-submitted for review.*

We are happy that the Reviewer found our approach for the calculation of the seismic response of ASSP walls interesting and hope that the detailed responses to the points above have clarified all the points raised by the Reviewer about our assumptions and results.

Reviewer 3

The authors present an interesting paper that adopts a limit equilibrium procedure for computing the yield acceleration of an anchored wall. They utilize Mononobe-Okabe earth pressure theory to define earth pressure coefficients for the soil pressures acting on the wall and anchor, and solve for yield acceleration by making several additional assumptions about the earth pressures below the dredge line. Their method is validated against a centrifuge modeling study from the literature, and against numerical simulations. I believe the paper is interesting and potentially useful for JGGE readers, but suggest that there are a number of deficiencies in the paper that should be addressed prior to publication.

Reviewer comment: 1. Figure 1. I was confused by the dashed lines at the top of the figure breaking up the length of the anchor. Why not just draw this as a continuous figure? Also, it is not clear why a pivot point should exist for the anchor. Isn't it possible that the anchor would translate to the left without rotating about a pivot?

The tie rod in Figure 1 was not drawn as a continuous line because Figure 1(a) refers to the assumed earth pressure distribution for $k_h < k_c$, *i.e.*, before a local plastic mechanism is attained into the system, whereas Figure 1(b) shows the contact pressure distribution on the anchor corresponding to full mobilisation of the capacity of the anchor, for the same value of k_h.

The kinematics of the anchor plate depends on the ratio b_A/H_A, representing the eccentricity of the anchor force with respect to the anchor plate. The condition $b_A/H_A = 2/3$ corresponds to a pure triangular distribution of the soil contact stresses, which is statically equivalent to the contact stress distribution for a pure translation of the anchor. We have tried to enhance this by showing schematically the contact stress distribution corresponding to different values of b_A/H_A in Figure 6. In general, the position of the pivot point (H_0), together with the anchor resistance (T_{lim}), is a result of the equilibrium of the anchor plate. In this sense, our assumption is more general and provides a more realistic prediction of T_{lim}. This point is further discussed as a comment to Figure 6 of the manuscript.

Reviewer comment: 2. Line 142: I suggest clarifying that KAE and KPE are the total earth pressures (static plus seismic) and not just the seismic increments. The Mononobe-Okabe method is most frequently formulated for the seismic increment, and readers could become confused by this.

We used the Mononobe-Okabe solution for K_{AE}, while the lower-bound solution proposed by Lancellotta (2007) was used to compute K_{PE}. We have slightly rewritten this part in the revised manuscript, in order to make it clearer (see also reply to Comment #9 raised by Reviewer #1).

Reviewer comment: 3. Line 144: I don't understand why the authors would assume that the pressure at a depth of D is equal to the pressure at the bottom of the wall. For typical cantilever walls, the pressure at the bottom of the wall is equal to the passive pressure on the retained side minus the active pressure on the other side. Why not stick with that assumption for consistency? Of course, the wall embedment depth, D, is then increased beyond the limit equilibrium depth to provide a factor of safety against passive failure of the embedded portion of the wall.*

We agree with the Reviewer that if the soil-wall contact is taken to be rigid-perfectly plastic and the wall to be rigid, for a cantilevered wall at failure, the "[…] pressure at the bottom of the wall is equal

to the passive pressure on the retained side minus the active pressure on the other side […]". However, Figure 1(a) refers to the assumed earth pressure distribution for a tied-back wall and for $k_h < k_c$, *i.e.*, before a local plastic mechanism is attained into the system.

As stated in the text, the pseudo-static earth pressure distribution assumed for the seismic design of tied-back walls was inspired by the work carried out by Conti & Viggiani (2013) and Conte *et al.* (2017) on embedded cantilever walls (see reply to Comments #8 and #9 raised by Reviewer #1). Both for tied-back walls and for cantilevered walls, the earth pressure distribution close to the bottom of the wall is affected by many factors, among which the soil-wall relative stiffness and the embedment depth, controlling the amount of wall displacement at the toe.

For typical cantilevered wall layouts and values of $k_h < k_c$, the soil close to the toe is far from being at limit state, as shown both numerically (Conti *et al.*, 2014) and theoretically (Conte *et al.*, 2017). When a tied-back wall attains failure this can happen either as failure of the retaining soil at the toe, and in this case the limit earth pressure distribution corresponds to that shown in Figure 7(a), or as a failure of the anchor, and, in this case, the limit earth pressure distribution will be similar to that shown in Figure 7(b), with a constant force, ($T_a = T_{lim}$) transmitted by the anchor to the wall. Although the overall kinematics resembles that of a failing cantilevered wall, in this case the strength of the soil at the bottom of the wall is not fully mobilised, neither on the active side nor on the passive side.

The earth pressure distribution proposed in this work was determined based on a preliminary study aimed at reproducing, even within a simple Limit Equilibrium framework, the actual distribution resulting from the soil-wall interaction. With reference to the general layout shown in Figure D, the assumption used in this work is $\sigma_2 = \sigma_1$, while the assumption suggested by the Reviewer and rigorously applicable to a cantilevered wall at failure is $\sigma_2 = \gamma \cdot K_{PE,h} \cdot (H+D) - \gamma \cdot K_{AE,h} \cdot D$. As expected, the two assumptions correspond to a different degree of mobilization of the soil passive pressure below dredge level (see Figure E) and therefore to a different bending moment distribution. This difference is significant in static conditions and reduces with increasing k_h, tending to zero as k_h tends to k_{TF}. Among the theoretical distributions explored in our preliminary study, the one characterised by the assumption $\sigma_2 = \sigma_1$ provides the best agreement with the numerical values obtained in this work.

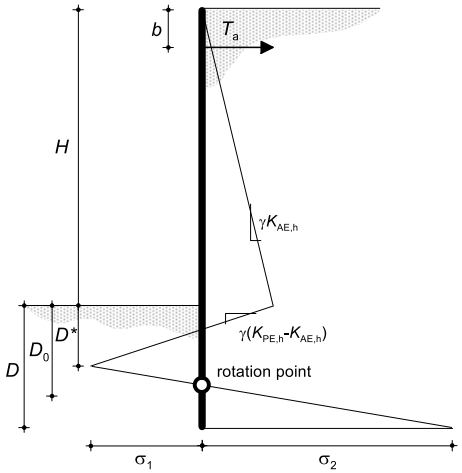

Figure D. General form of the net earth pressure distribution assumed in the proposed pseudo-static limit equilibrium method.

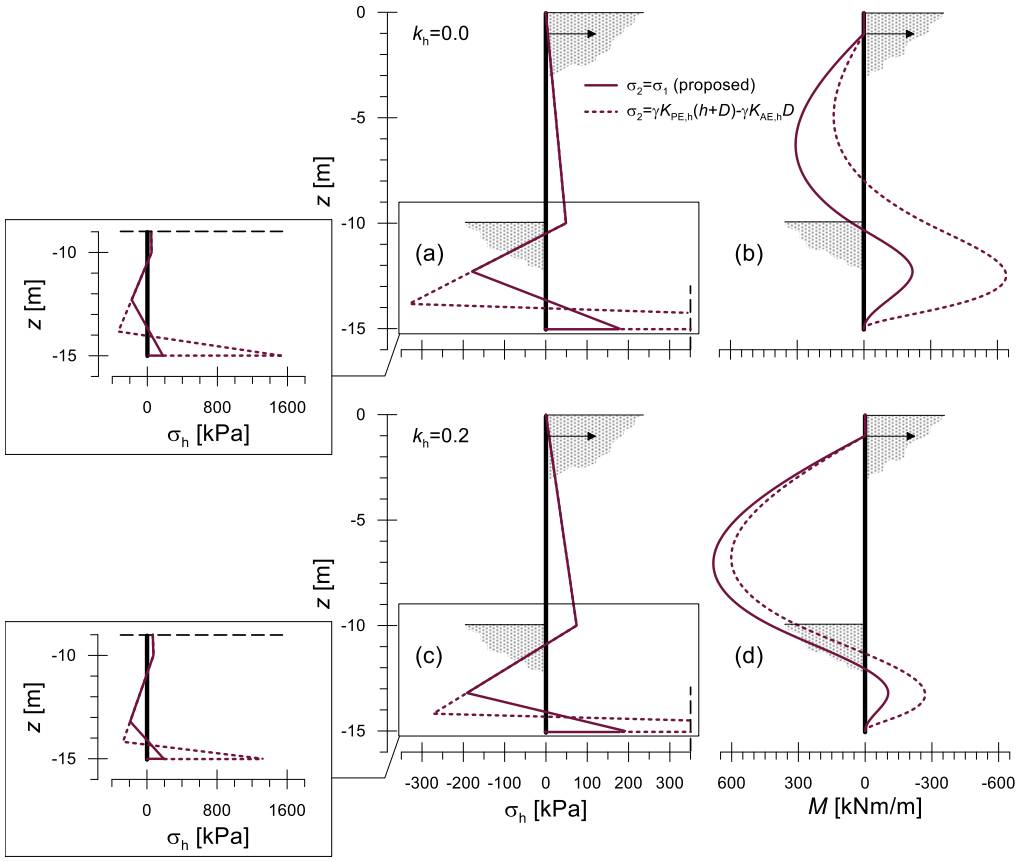

Figure E. Comparison between two possible earth pressure distributions, in terms of: horizontal contact stress (a, c) and bending moment (b, d).

<u>Reviewer comment:</u> 4. Figure 2: The abrupt transition of earth pressure at the rotation point in Fig. 2b is generally considered unrealistic. This would be correct based on the assumption of rigid-perfectly plastic material behavior (an assumption inherent to limit equilibrium methods), but is not reasonable for elasto-plastic material behavior. Generally a line is drawn from the bottom of the pressure distribution through the rotation point to a point where the line intersects the pressure distribution on the other side of the wall. See the US Steel Sheet Pile manual, for example, for the shape of this distribution.

We agree with the Reviewer that the jump in the earth pressure distribution at the rotation point in Fig. 2b is unrealistic, but this is what is proposed in Method M2, taken from the literature (see also reply to Comments #10 and #12 raised by Reviewer #1). Regarding the distribution suggested by the Reviewer, please see the reply to Comment #3.

<u>Reviewer comment:</u> 5. Line 393: The authors mention the use of Newmark sliding block analysis in conjunction with their proposed limit equilibrium method for computing yield acceleration. However, it seems out of place here. I suggest that a separate paper focusing on permanent wall deformations would be a better venue for discussing the Newmark sliding block procedure. It is not clear to me that such a procedure would work well considering the flexibility of the system (note that Newmark sliding block procedures assume a rigid sliding mass).

Acknowledged. Reference to the possible application of our results also for the computation of seismic induced permanent displacements, using a Newmark's type analysis, has been removed in the revised manuscript, both in the Abstract and Conclusions. Indeed, we are currently working on

this topic and we agree with the Reviewer that application of the Newmark's procedure to embedded ASSP walls is still an open issue, given the multiple factors affecting their seismic behaviour. This point is explicitly addressed in the Introduction of the manuscript (see also reply to Comment #2 raised by Reviewer #1).

Reviewer comment: 6. The authors compared their proposed procedure with results from numerical modeling studies that utilized a pseudo-static body force to model horizontal shaking intensity. This misses a large number of features of real earthquake ground motions, including wave propagation and soil-structure interaction. It is unclear to me why the authors adopted a pseudo-static method to validate their approach when they could have utilized real ground motions instead. More justification is required in the paper for this approach.

Numerical pseudo-static (pushover) analyses are a powerful tool to identify the plastic mechanisms within a soil-structure system and the related yield accelerations. As such, they were recently adopted to study the mechanical response of different types of retaining structures (Callisto, 2014; Masini *et al*., 2015; Conti & Caputo, 2019).

We agree with the Reviewer that numerical pseudo-static analyses miss (in general) a number of features of real earthquakes, including wave propagation (possible phase-shift and amplification of soil accelerations) and soil-structure interaction effects. However, the relative importance of such features depends on the characteristics of the geotechnical system under investigation. In the case of yielding walls, including ASSP walls, the onset of plastic mechanisms within the soil-structure system makes the dynamic interaction problem a strength-driven rather than a deformability-driven problem. Moreover, given the typical values of wall height (H < 20 m) and soil shear wave velocity (V_s = 150-250 m/s), phase shift of soil accelerations is not expected to have a significant effect during real earthquakes. Based on these considerations, pseudo-static analyses have been proven to provide relevant information on the behaviour of retaining structures during real earthquakes and on their seismic design (Conti & Caputo, 2019).

As outlined in the Introduction of the manuscript, in modern codes and guidelines for design, the seismic performance of retaining structures is typically assessed in terms of permanent displacement. However, any simplified procedure for the computation of seismic permanent displacements must be validated against either physical models and real case studies or numerical fully dynamic analyses. As our study focuses on the overall seismic behaviour of ASSP walls, with the aim of defining simplified procedures for their seismic design, we were conducting both pseudo-static and fully dynamic numerical analyses.

The original idea was to separate the discussion on the pseudostatic behaviour of ASSP walls, focusing on the activation of plastic mechanisms and the computation of internal forces in the structural members, from the analysis of their dynamic behaviour during real earthquakes, focusing essentially on the progressive accumulation of permanent displacements. However, we agree with the Reviewer that a comparison between pseudo-static and dynamic numerical results can provide valuable information on the overall dynamic behaviour of ASSP walls and on their structural design, and strengthens some of the conclusions of our original work.

Therefore, the revised manuscript has been modified to include also the results of a number of fully dynamic numerical analyses, carried out using the FDM code FLAC. The four layouts of ASSP walls were subjected to six real earthquakes, covering a wide range of amplitudes and frequency contents.

Moreover, for layouts #1, #2 and #3, further dynamic analyses were carried out by scaling the applied inputs to lower values of the maximum acceleration, in order to investigate the response of the anchor-wall system under lower-intensity seismic excitations. The relevant features of the numerical model are defined in Section 3.2, while the main results are discussed in Section 4.2 of the revised manuscript.

References

Andrianopoulos, K. I., Papadimitriou, A. G., Bouckovalas, G. D. (2010a). "Bounding surface plasticity model for the seismic liquefaction analysis of geostructures". *Soil Dyn Earthq Eng* 30(10):895–911.

Andrianopoulos, K. I., Papadimitriou, A. G., Bouckovalas, G. D., (2010b). "Explicit integration of bounding surface model for the analysis of earthquake soil liquefaction". *International Journal for Numerical and Analytical Methods in Geomechanics*. 34, 1586-1614.

ArcelorMittal (AM) Manual. (2009). "Foundation Solutions for Projects. Harbour Construction. Innovative steel sheet pile solutions for modern ports".

Bilgin, Ö. (2010). "Numerical Studies of Anchored Sheet Pile Wall Behavior Constructed in Cut and Fill Conditions". *Computers and Geotechnics* 37 (3): 399–407.10.1016/j.compgeo.2010.01.002.

Bilgin Ö. (2012). "Lateral Earth Pressure Coefficients for Anchored Sheet Pile Walls". *International Journal of Geomechanics*. 12(5) 584-595.

Biondi, G., Cascone, E., & Maugeri, M. (2014). "Displacement versus pseudo-static evaluation of the seismic performance of sliding retaining walls". Bulletin of Earthquake Engineering, 12(3), 1239-1267.

Callisto, L., Soccodato, F. M. & Conti, R. (2008). "Analysis of the seismic behaviour of propped retaining structures". In Geotechnical earthquake engineering and soil dynamic IV (eds D. Zeng, M. T. Manzari and D. R. Hiltunen), GSP 181, pp. 1–10. Reston, VA, USA: ASCE.

Callisto, L. & Soccodato, F. M. (2010). "Seismic design of flexible cantilevered retaining walls". *J. Geotech. Geoenviron. Engng* 136, No. 2, 344–354.

Callisto, L. (2014). "Capacity design of embedded retaining structures". *Géotechnique*, 64(3), 204-214.

Callisto, L. (2019). "On the seismic design of displacing earth retaining systems". Proceedings of the 7th International Conference on Earthquake Geotechnical Engineering, (ICEGE 2019), June 17-20, 2019, Rome, Italy. CRC Press.

Cilingir, U., Haigh, S. K., Madabhushi, S. P. G., & Zeng, X. (2011). "Seismic behaviour of anchored quay walls with dry backfill". *Geomechanics and Geoengineering*, 6(3), 227-235.

Cattoni, E., Salciarini, D., Tamagnini, C. (2019). "A Generalized Newmark Method for the assessment of permanent displacements of flexible retaining structures under seismic loading conditions". *Soil Dyn. Earthq. Eng*. 2019, 117, 221–233.

Conti, R. (2010). "Modellazione fisica e numerica del comportamento di opere di sostegno flessibili in condizioni sismiche".

Conti, R., Madabhushi, G. S. P., & Viggiani, G. M. B. (2012). "On the behaviour of flexible retaining walls under seismic actions". *Géotechnique*, 62(12), 1081-1094.

Conti, R. (2017). “Numerical modelling of centrifuge dynamic tests on embedded cantilevered retaining walls”. Italian Geotechnical Journal - Rivista Italiana di Geotecnica, 51(2), 31-46.

Conti, R., & Viggiani, G. M. (2013). “A new limit equilibrium method for the pseudo-static design of embedded cantilevered retaining walls”. *Soil Dynamics and Earthquake Engineering*, 50, 143-150.

Conti, R., Madabhushi, G. S. P., Mastronardi V. & Viggiani, G. M. B. (2015). “Centrifuge dynamic tests on gravity retaining walls: an insight into bearing vs sliding failure mechanisms”. Proc. 6th Int. Conf. Earthquake Geotech. Eng., Christchurch, New Zealand.

Gazetas, G., Garini, E., & Zafeirakos, A. (2016). “Seismic analysis of tall anchored sheet-pile walls”. *Soil Dynamics and Earthquake Engineering*, 91, 209-221.

Masini, L., Callisto, L., & Rampello, S. (2015). “*An interpretation of the seismic behaviour of reinforced-earth retaining structures*”. *Géotechnique*, 65(5), 349-358.

NTC, L. G. (2008). Norme tecniche per le costruzioni. Italian technical norms for constructions.

Roeder, C.W., Lehman, D.E., Yoo, J.H. (2005). “Improved seismic design of steel frame connections”. *Steel structures*, 5, 141-153.

Steedman, R. S. (1998). “Seismic design of retaining walls”. Proceedings of the Institution of Civil Engineers-Geotechnical Engineering, 131(1), 12-22.

Sugano, T., Nozu, A., Kohama, E., Shimosako, K. I., & Kikuchi, Y. (2014). “Damage to coastal structures”. *Soils and Foundations*, 54(4), 883-901.

Sumer, B. M., Ansal, A., Cetin, K. O., Damgaard, J., Gunbak, A. R., Hansen, N. E. O., ... & Zen, K. (2007). “Earthquake-induced liquefaction around marine structures”. Journal of waterway, port, coastal, and ocean engineering, 133(1), 55-82.

Towhata, I., & Islam, M. S. (1987). “Prediction of lateral displacement of anchored bulkheads induced by seismic liquefaction”. *Soils and foundations*, 27(4), 137-147.

Zeng, X., & Steedman, R. S. (2000). “Rotating block method for seismic displacement of gravity walls”. *Journal of Geotechnical and Geoenvironmental Engineering*, 126(8), 709-717.